Noname manuscript No.
(will be inserted by the editor)

Helical birods: An Elastic Model of Helically Wound Double-Stranded Rods

Christopher Prior

Received: date / Accepted: date

Abstract We consider a geometrically accurate model for a helically wound rope constructed from two intertwined elastic rods. The line of contact has an arbitrary smooth shape which is obtained under the action of an arbitrary set of applied forces and moments. We discuss the general form the theory should take along with an insight into the necessary geometric or constitutive laws which must be detailed in order for the system to be complete. This includes a number of contact laws for the interaction of the two rods, in order to fit various relevant physical scenarios. This discussion also extends to the boundary and how this composite system can be acted upon by a single moment and force pair. A second strand of inquiry concerns the linear response of an initially helical rope to an arbitrary set of forces and moments. In particular we show that if the rope has the dimensions assumed of a rod in the Kirchhoff rod theory then it can be accurately treated as an isotropic inextensible elastic rod. An important consideration in this demonstration is the possible effect of varying the geometric boundary constraints; it is shown the effect of this choice becomes negligible in this limit in which the rope has dimensions similar to those of a Kirchhoff rod. Finally we derive the bending and twisting coefficients of this effective rod.

Keywords Cosserat Rods · Contact Mechanics · Ropes · Constitutive Law · Lock-Up

Mathematics Subject Classification (2000) 74B15 · 74B20 · 74Q15 · 74M15

1 Introduction

A common structure in both engineering applications and biology is the intertwined helical motif one would associate with ropes (see Figure 1(a)). From an engineering perspective wire ropes are used to stabilise bridges and oil platforms, as well as being used in mine-shafts for raising and lowering resources. As shown in Figure 1(b) the cross-sectional structure of these ropes can be highly elaborate, composed of multiple scales of inter-wound structure. For example the third of Figure 1(b) is composed on its largest scale of six ropes surrounding a single rope, but each of these ropes then has a further sub-structure, which in this case happens to have the same form as the larger scale. In human biology perhaps the most widely recognised example would be the DNA double helix. However, there are a myriad of fibrous proteins with similar or more complex inter-wound cross-sectional structure such as keratins, collagens, elastins and intermediate filaments. Such structures form a vital component of cytoskeletal structures and are used in a number of biological processes [36], including forming parts of molecular motors [28]. Whilst recognising the inadequacy of a single word to cover the variety of systems that exhibit this inter-wound structure, we shall use the term rope as a convenient short-hand.

Department of Mathematical Sciences, Durham University, Science Laboratories, South Rd, Durham, United Kingdom, DH1 3LE
+44-(0)191-334-3050
E-mail: christopher.prior@durham.ac.uk

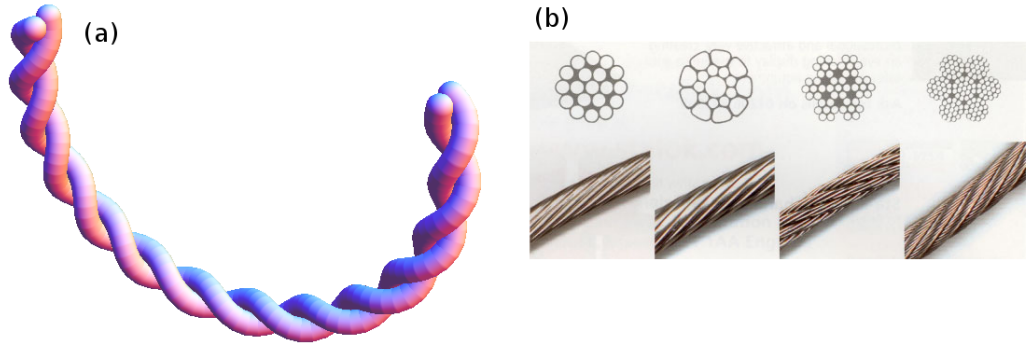

Fig. 1 Figures depicting examples of the type of rope structure we are interested in. Panel (a) depicts perhaps the simplest example of what we term a rope in this note, composed of two helically inter-wound tubes, this figure was plotted using the model we derive in this note and could be used as an elastic model for DNA molecule. In panel (b) we see examples of wire ropes and their complex cross-sectional structure. We see there are a number of scales of structure.

There is significant interest in the mechanical properties of ropes in the engineering field. There are a number of common modes of failure in ropes including snapping of individual strands, the unfolding of the contacting structure commonly referred to as bird-caging and bucking, which occurs when the straightened rope structure bends leading to a loss of the tautness required to provide stability. In biopolymers many vital functional behaviours of rope biopolymers require that they be bent, folded and twisted, and there is significant interest in their mechanical response under stress [22,23,35,38,40,42].

A popular modelling tool for such ropes has been to treat the individual elements as thin tubular continua, namely (Cosserat) rods (*e.g.*, [11,29,48]). By individual elements we mean the smallest scale of structure for which there is no further macroscopic cross-sectional structure (*i.e.*, in Figure 1(a) there are two such continua composing the rope structure, in Figure 1(b) there would be many more). This as opposed to treating the composite whole as a continuum [14,19,34], an approach that can greatly simplify the modelling but which would omit vital aspects of a rope's mechanical response. In particular, the finite volume of individual elements of the rope leads to geometric constraints relating the fact that individual elements will often be in contact with each other, and it must be ensured that they cannot overlap when deformed. In modelling terms this has the dual purpose of preventing non-physical configurations of the rope and also to allow for the correct descriptions of the mutual contact forces induced between the elements as a result of the deformation. For mechanical ropes this interaction is an obvious function of the solid material structure of the individual rope elements. For biopolymers this excluded volume effect is due to the mutual repulsion of the electron density composing the individual elements of the rope composite. There is significant evidence to suggest that this approximate tube model for biopolymers is a relevant one as it has been used with success in a number of studies (a few examples amongst many are [4–8,39,49]).

A notable consequence of this finite volume effect is the fact it is physically impossible to tighten a rope structure by increasing the helical pitch (rate of winding) indefinitely, as we would eventually encounter a self-intersecting structure [29]. For the case in which we have two inter-wound tubular this phenomenon has been termed *lock-up* [29,31]. It was demonstrated in [29,43,47] that this results in the mathematical divergence of the mutual pressure exerted in individual rods as the rope is helically tightened towards this limit. This phenomenon would not naturally be captured by a single continuum model.

We make a point of highlighting this issue of the geometry of mutual contact of rope elements as it has not always been fully addressed in the literature. There has been a significant body of work in the engineering literature which concerns the development of models of wire ropes (see [13] for a brief review). In this approach the individual strands of the rope are treated using rod theory. The individual strands are modelled by considering an individual rod whose undeformed geometry is helical and using the equations of equilibrium to determine the change in shape of the centreline of rotation under a set of applied forces and moments. In a well cited study by Costello [10], a measurement of the effective bending stiffness of a helical rod was determined, *i.e.*, a measure of the moment required to turn the initially straight helical shape into that of a curve winding on a section of a torus whose curvature is the measure of its bending. This measure is then assumed to apply to each individual rod of a full wire structure, and some (incorrect) geometric assumptions based on the geometry of the cross-sections of the rope's individual elements are then used to build a composite model for the full structure [11,48]. A significant downside to this approach was the lack of consideration of body forces imposed on the

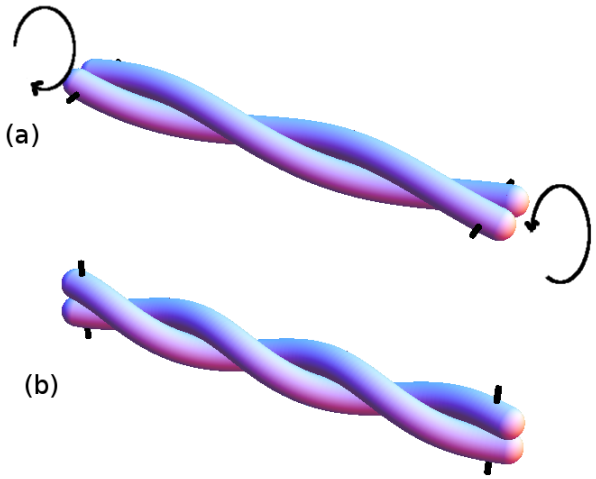

Fig. 2 A depiction of a pinning device used to apply a single torque to a rope constructed from two rods. By turning the pin about the rope's centre as shown in (a) a set of forces and moments will be applied to the individual rods causing their change in shape depicted in (b).

individual rods by their contacting neighbours. In subsequent work [24,32,33], both contact forces and moments were considered, though once again the studies only modelled an isolated helical rod, rather than considering the whole system in a single model. A number of authors have proposed various extensions or variations on this model [2,16,20,37] but they rely on the same geometric assumptions of elliptic cross-sections, which is not in general correct even if the rope remains unbent (see *e.g.*, [29]). Alternative models make ad hoc assumptions regarding the kinematics of the constituent rods [12,46], but none of these works correctly treat the contact problem.

On the applied mathematics side, various studies have addressed these issues by coupling the individual rod equations of each strand by correctly treating the contact geometry of the structure [29,43,47]. These works considered the case in which the rods were helical and did not consider bending of the structure. This approach is shown to lead to the divergence of forces as lock up was approached. Neukirch and van der Heijden [29] considered n intertwined helical rods, this approach has recently been extended to include a compressible rod in the centre of the structure [27]. The natural extension of this approach would be to allow for the structure to bend under the action of moments and forces, it is this problem which we shall begin to address in this work and subsequent studies. The aim is to first treat the smallest scale of structure of the rope structure as a single rod so that the next scale can then be treated in the same manner. In this particular study we limit ourselves to the case of two rods which have initially a single line of contact, following [26] we call this a birod. Treating this simpler case proves to be of significant difficultly in and of itself, however, many of the issues confronted in this study will naturally carry over to the n rod case. In particular the framework for defining the interaction mechanics of contacting rod elements which we develop.

A study by Moakher and Maddocks [26] considered a variant of this problem in the case for which the two rods composing the birod were stuck together, forbidding relative motion of the two composing rods such as the relative sliding an twisting of the two rods with respect to each other. Such a model would be relevant for a system such as a DNA molecule where the base pairs of the two polypeptide strands are paired by covalent bonds. On the other hand many coiled-coil structures interact relatively weakly through Van-Der-Waals forces and hydrophilic interactions which would not greatly restrict such motions. Also, mechanical ropes are often lubricated such that they are relatively free to slip without much fictional wear. Starostin and van der Heijden [41] considered the equilibria of a birod model in which the rods are free to slide. Still more generally one might also need to consider the presence of frictional forces in the rope interactions in dynamic studies. It is clear that a more general model is necessary to allow for a significant range of possible interaction laws. In this note we propose such a model and discuss the possible mathematical means for specifying the interactions law of the two rope strands in section (3.2). This could be geometrically such as in [26] or through constitutive laws specifying the mechanical interaction through contact of the two structures. By making explicit assumptions about the shape and density of the constituent rods, namely that they are circular and unstretchable, we make this model relatively simple and tractable.

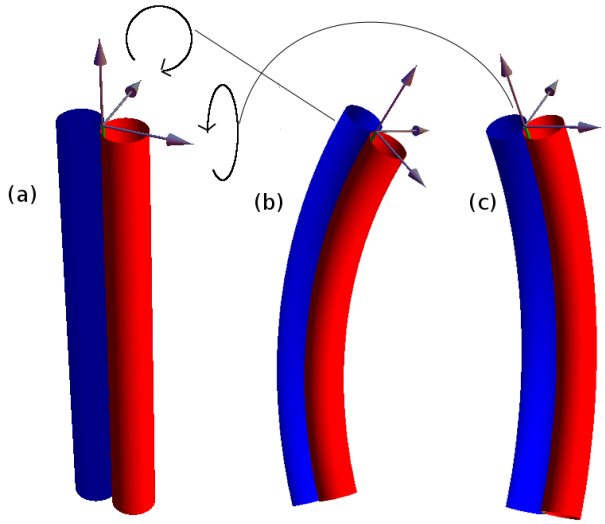

Fig. 3 Depiction of the bending asymmetry of a birod. Panel (a) depicts an un-bent birod, the tangent vector of their line of contact and two vectors in its normal plane. The first points towards the centre of one of the rods the other is perpendicular. In (b) we see the effect of applying a bending moment about the second direction, on this case the two rods are caused to press against each other leading the pair to bend. In (c) we see the effect of applying a bending moment about the direction point towards the rod's centre. We see the two rods bend mutually without having to press against each other.

A second aspect of this study concerns the means by which we can apply forces and moments to a rope in the same manner we do to individual rods; this functionality would be particularly useful for creating composite models of a series of ropes (hierarchical models). For a single rod we apply a force/moment combination (a wrench) to each end of the rod as the boundary conditions. In practice we can apply a single wrench force as the ends of a birod if it is in some way glued or bound at its ends, as shown with an imagined pinning device depicted in (Figure 2). Turning the pin will naturally impart individual forces on the two rods by restricting their individual motions with respect to each other and we have a means of treating the system as a single rod.

A second consideration in the attempt to treat a rope as a rod would be to develop a simple constitutive law for the rope with the same mathematical structure as that use for a single Cosserat rod, in particular the linear constitutive law which relates the moments about the rod cross-sections to its local degree of bending and twisting through constant values. For isotropic circular rods the moment required to bend about any particular axis does not vary. However, even for birods composed of circular rods we might expect a pronounced asymmetry as applying a moment about one direction could correspond to pressing the rods into each other (Figure 3(a)) or bending about the same direction without needing to press against each other, (Figure 3(b)). Studies by Kehrbaum and Maddocks [21] , and Healey [19], found linear laws could be recovered for single birods which had the assumed symmetry of helical birods. However, this work neglects the non linear effects one would expect to result from the diverging pressure due to lock-up. Neukirch and van der Heijden [29] derived constants for the torsional response of a birod which did take into account this divergence. The aim of this study is to extend this work to more general geometries to obtain coefficients for the bending of the birod.

In Section 2 we discuss the governing kinematics of the birod. In Section 2.4 we show how the kinematics of the individual rods can be expressed in terms of the kinematic parameters of the contact line.

In Section 3 we discuss the balance equations of the birod structure (22-25). We discuss the five degrees of kinematic freedom inherent to the birod structure, on which it is necessary to impose constraints in order to complete the system. Finally we discuss the application of the boundary conditions through the imposition of geometric constraints.

In Section 4 we derive and discuss the equilibrium state of a birod composed of helically intertwined rods whose contact line is straight. In particular the state in which the composite birod force and moment are zero so it will act as our undeformed effective rod.

In Section 5 we detail the linearisation procedure used to obtain the linear response of the birod. This is based on the perturbation scheme of Goriely and Tabor [17].

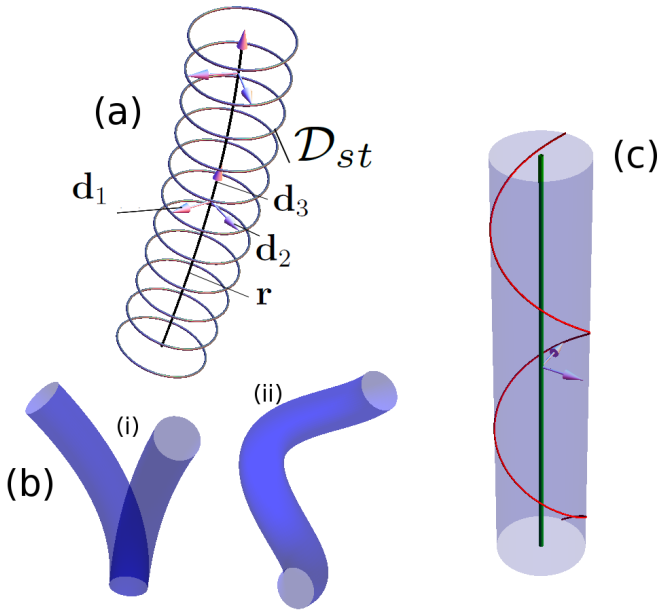

Fig. 4 Depictions of various aspects of the rod construct. In (a) we see a visualisation of the set of discs $\mathcal{D}_{st}$ which constitute the rod body. Also shown is the director basis. In (b)(i) we see two example rods which have curvature but not torsion, they bend in planes. The rod depicted in (ii) contorts out of plane due to the rotation of the Frenet frame, it has torsion. The red curve in (c) depicts the additional twisting of the basis, which used to represent the degree of freedom offered by the relative rotation of the material discs $\mathcal{D}_s$ under the action of a torque.

In section 6 we discuss the solutions of the system. In particular we focus the relationship between the birod's total force and moment and the curvatures of the contact line. We derive the linear bending coefficients and twisting coefficients in the limit in which the ratio L/R, the length L and radius R of the birod, is large, as well as discussing the suitability of these approximations. We show these results can be used to obtain previous torsional and axial strain constitutive behaviour found in [29].

Finally in section 7 we review the results obtained.

2 Kinematics and Dynamics of the Model

2.1 Cosserat Rods

A birod is composed of a pair of unshearable, inextensible, elastic Cosserat rods. A Cosserat rod is defined by a pair of vector fields $[0, L] \times \mathbb{R} \to \mathbf{r}(s,t), \mathbf{d}_1(s,t) \in \mathbb{E}^3$. The position vector $\mathbf{r}$ represents the location of the rod central axis in a Cartesian reference frame $(\hat{\mathbf{x}}, \hat{\mathbf{y}}, \hat{\mathbf{z}})$. It is required to be least three times differentiable on the interval $s \in [0, L]$ and twice differentiable with respect to t. A moving right-handed orthonormal basis of $\mathbb{E}^3$, the *director basis*, is defined for the rod using the position vector's unit tangent vector $\mathbf{d}_3(s,t)$, $||\mathbf{d}_3|| = 1$, and the unit vector field $\mathbf{d}_1(s,t)$ which lies in the normal plane of $\mathbf{r}$ ($\mathbf{d}_1 \cdot \mathbf{d}_3 = 0$, $||\mathbf{d}_1|| = 1$, $\forall s, t$). The basis is completed by the vector product $\mathbf{d}_2 = \mathbf{d}_3 \times \mathbf{d}_1$. Usually for Cosserat rod models the parameter s is chosen to be the arclength of the curve $\mathbf{r}$, for which $||\, \mathrm{d}\mathbf{r}/\, \mathrm{d}s|| = 1$ [25], however, in what follows we must use a parametrisation for the rod which is not its arclength, so that $||\, \mathrm{d}\mathbf{r}/\, \mathrm{d}s|| = \lambda(s,t)$, which slightly changes some of the usual kinematic expressions.

The Cosserat theory is a one dimensional model of a thin three-dimensional body, composed from a set of planar material cross-sections attached to the axis curve $\mathbf{r}$ (see *e.g.*, [1]). Usually the specific geometry of the cross-sections is not explicitly characterised, however, in this work the exact dimensions of the rod will form a vital part of the birod inter-wound geometry. For this birod model we require the cross-sections to be circular discs with constant radius R. At a specific parameter value s the pair $(\mathbf{d}_1, \mathbf{d}_2)$ span the circular cross-section

$\mathcal{D}_{st}$ whose material points $\mathbf{p}$ are specified by the pair (r, ξ) with

$$P_{s,t}(r,\xi) = \mathbf{r}(s,t) + r(\mathbf{d}_1(s,t)\cos(\xi) + \mathbf{d}_2(s,t)\sin(\xi)),$$

and $\mathcal{D}_{st} = \left\{P_{s,t}(r,\xi) | r \in [0,R], \xi \in S^1\right\}$. The set of all $\mathcal{D}_{st}$ on the interval $s \in [0,L]$ constitutes the rod body at a time t, as depicted in Figure 4(a).

Particular configurations of the rod can be characterised by the evolution of the basis $\{\mathbf{d}_i\}$ with s and t via the differential equations

$$\mathbf{d}_j' = \lambda \mathbf{u}(s) \times \mathbf{d}_j(s), \quad \dot{\mathbf{d}}_i = \mathbf{w}(s) \times \mathbf{d}_j(s), \ j = 1,2,3, \tag{1}$$

where the prime denotes partial differentiation w.r.t s, the dot partial differentiation w.r.t time t, and the axial vectors $\mathbf{u}$ (the *strain* vector) and $\mathbf{w}$ (the *spin* vector) are defined using six differentiable scalar functions $\mathsf{u}_j(s,t)$ and $\mathsf{w}_j(s,t)$, such that

$$\mathbf{u} = \mathsf{u}_1\mathbf{d}_1 + \mathsf{u}_2\mathbf{d}_2 + \mathsf{u}_3\mathbf{d}_3, \quad \mathbf{w} = \mathsf{w}_1\mathbf{d}_1 + \mathsf{w}_2\mathbf{d}_2 + \mathsf{w}_3\mathbf{d}_3.$$

Hereafter the components of a vector $\mathbf{v}$ in the director basis will always be written in the Sans-Serif font v_j, $j = 1,2,3$. With this we have two linear systems of ordinary differential equations

$$\begin{pmatrix} \mathbf{d}_1' \\ \mathbf{d}_2' \\ \mathbf{d}_3' \end{pmatrix} = \lambda \begin{pmatrix} 0 & \mathsf{u}_3 & -\mathsf{u}_2 \\ -\mathsf{u}_3 & 0 & \mathsf{u}_1 \\ \mathsf{u}_2 & -\mathsf{u}_1 & 0 \end{pmatrix} \begin{pmatrix} \mathbf{d}_1 \\ \mathbf{d}_2 \\ \mathbf{d}_3 \end{pmatrix}, \quad \begin{pmatrix} \dot{\mathbf{d}}_1 \\ \dot{\mathbf{d}}_2 \\ \dot{\mathbf{d}}_3 \end{pmatrix} = \begin{pmatrix} 0 & \mathsf{w}_3 & -\mathsf{w}_2 \\ -\mathsf{w}_3 & 0 & \mathsf{w}_1 \\ \mathsf{w}_2 & -\mathsf{w}_1 & 0 \end{pmatrix} \begin{pmatrix} \mathbf{d}_1 \\ \mathbf{d}_2 \\ \mathbf{d}_3 \end{pmatrix}. \tag{2}$$

The requirement that the partial derivatives of $\mathbf{d}_j$ commute in s and t lead to the following compatibility conditions

$$\mathbf{w}' - \dot{\mathbf{u}} = \mathbf{u} \times \mathbf{w}. \tag{3}$$

[17]. For given vectors $\mathbf{u}(s,t)$ and $\mathbf{w}(s,t)$, length L, radius R and function λ, a rod's configuration is defined at all t by the solutions of (2), up to a global translation and rotation determined by the initial conditions.

For our birod model we will know the functions $\mathbf{r}$ of each rod as a function of the kinematic variables of the line of their mutual line of contact (defined in Section 2.2). The aim is to express the kinematics of the individual rods in terms of these variables through the expression for $\mathbf{r}$. The functions u_j and w_j can be expressed as functions of $\mathbf{r}$ via the Frenet framing, which is defined through the *Normal* vector $\boldsymbol{\nu} = \mathbf{d}_3'/||\mathbf{d}_3||$ and *Binormal* vector $\boldsymbol{\beta} = \mathbf{d}_3 \times \boldsymbol{\nu}$, with

$$\boldsymbol{\nu} = \frac{\mathbf{r}' \times (\mathbf{r}^{''} \times \mathbf{r}')}{||\mathbf{r}'||\,||\mathbf{r}_i' \times \mathbf{r}_i^{''}||}, \quad \boldsymbol{\beta} = \frac{\mathbf{r}' \times \mathbf{r}^{''}}{||\mathbf{r}' \times \mathbf{r}''||}, \tag{4}$$

[25]. The Frenet frame satisfies the differential equation

$$\begin{pmatrix} \boldsymbol{\nu}' \\ \boldsymbol{\beta}' \\ \mathbf{d}_3' \end{pmatrix} = \lambda \begin{pmatrix} 0 & \tau & -\kappa \\ -\tau & 0 & 0 \\ \kappa & 0 & 0 \end{pmatrix} \begin{pmatrix} \boldsymbol{\nu} \\ \boldsymbol{\beta} \\ \mathbf{d}_3 \end{pmatrix}. \tag{5}$$

with the *curvature* κ and *torsion* τ given by

$$\kappa = \frac{||\mathbf{r}' \times \mathbf{r}''||}{||\mathbf{r}'||^3}, \quad \tau = \frac{(\mathbf{r}' \times \mathbf{r}'') \cdot \mathbf{r}'''}{||\mathbf{r}' \times \mathbf{r}''||^2}. \tag{6}$$

In order to properly represent the independent degree of freedom of axial rotation of the material discs about $\mathbf{d}_3$ we define a function $\phi(s,t)$, which parametrises an additional rotation of the pair $(\boldsymbol{\nu}, \boldsymbol{\beta})$ about $\mathbf{d}_3$ to obtain the director basis, *i.e*,

$$(\mathbf{d}_1, \mathbf{d}_2) = (\cos(\phi)\boldsymbol{\nu} + \sin(\phi)\boldsymbol{\beta}, -\sin(\phi)\boldsymbol{\nu} + \cos(\phi)\boldsymbol{\beta}). \tag{7}$$

Taking partial derivatives of $\mathbf{d}_j$ with respect to s, using (5) and comparing to (2) we have

$$\mathsf{u}_1 = \kappa\sin(\phi), \quad \mathsf{u}_2 = \kappa\cos(\phi), \quad \mathsf{u}_3 = \tau + \frac{\phi'}{\lambda}. \tag{8}$$

Finally, by differentiating (7) with respect to t and using the relations

$$\mathsf{w}_1 = \mathbf{d}_3 \cdot \dot{\mathbf{d}}_2, \quad \mathsf{w}_2 = -\mathbf{d}_3 \cdot \dot{\mathbf{d}}_1, \quad \mathsf{w}_3 = \mathbf{d}_2 \cdot \dot{\mathbf{d}}_1, \tag{9}$$

we can obtain the components of the spin vector in terms of partial derivatives of $\mathbf{r}$.

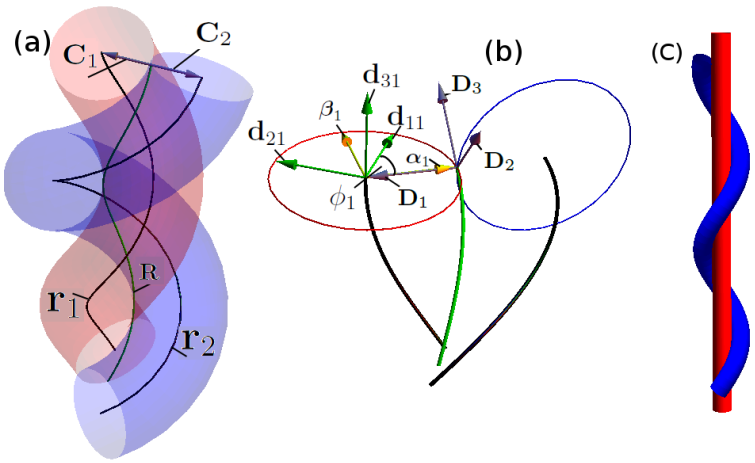

Fig. 5 (a) two intertwined Cosserat rods with centre lines $\mathbf{r}_1$ and $\mathbf{r}_2$ and a mutual line of contact $\mathbf{R}$. The vectors $\mathbf{D}_1$ and $\mathbf{D}_2$ which are used to characterise the rod geometry in terms of the contact line geometry are shown. (b) the various framing's used to characterise the birod's kinematics (in this case we see the kinematics of rod $\mathbf{r}_1$). The contact frame $(\mathbf{D}_3, \mathbf{D}_1, \mathbf{D}_2)$ is shown. Also shown is the Frenet framing $(\mathbf{d}_{31}, \boldsymbol{\nu}_1, \beta_1)$ and the angle ϕ_1 between the vector $\mathbf{d}_{11}$ and $\boldsymbol{\nu}$. Note that the normal vector and $\mathbf{D}_1$ overlap. This is not generally true but is its true for the un-deformed double helix state we use in Section 4. (c) a birod configuration which is not allowed by our definition as one of the rods has sections with no contact.

2.2 Birod Kinematics and Dynamics

We consider two intertwined Cosserat rods with the same cross-sectional radius R and whom share a mutual line of contact which we label $\mathbf{R}(s,t)$ (Figure 5(a)). This contact line $\mathbf{R}(s,t)$ inherits its differentiability from the rod centrelines. In what follows all vectors positioned on the contact line will be capitalised, as will their components. We do not make any assumptions about the particular form of the kinematic parametrisation s used for the contact line at this stage, but will discuss some of the possible choices in due course. It is the parameter s which we now identify as that used in the previous section and we now explain how it can be used to parametrise the individual constituent rods, irrespective of the specific choice of kinematic parametrisation. We label the rods $1, 2$ with subscripts $(\mathbf{r}_1, \mathbf{r}_2)$. The rods may have differing arc lengths L_1 and L_2 but we require there is no section of either rod which is not in contact with the other (ruling out configurations such as shown in Figure 5(c)). To be more precise, each point $\mathbf{R}(s)$ will be in contact with of two unique material discs $\mathcal{D}_1(s_1(s,t))$, of rod 1 and $\mathcal{D}_2(s_2(s,t))$ of rod 2, with the functions $s_1(s,t)$ and $s_2(s,t)$ the arc lengths of rods 1 and 2 respectively. Note that even if the rods have the same length the requirement that the rods are in continual contact does not imply $s_1(s,t) = s_2(s,t)$, $\forall s$. We also do not necessarily require that two discs in contact at a time t are in contact with each other at any other time, except the end disc pairs $(\mathcal{D}_1(s_1(s_{min},t)), \mathcal{D}_2(s_2(s_{min},t))$ and $(\mathcal{D}_1(s_1(s_{max},t)), \mathcal{D}_2(s_2(s_{max},t))$, which remain paired for all t.

We now define two vectors $\mathbf{C}_i(s,t)$ which join the centrelines of the rods $\mathbf{r}_1$ and $\mathbf{r}_2$ to the contact curve $\mathbf{R}$ as

$$\mathbf{r}_i(s,t) = \mathbf{C}_i(s,t) + \mathbf{R}(s,t).$$

The vectors, depicted in Figure 5(a), are always anti-parallel *i.e.*, $\mathbf{C}_1 = -\mathbf{C}_2$.

Indeed we are considering the contact to two convex shapes (sections of a tube which are locally cylindrical) so their tangent planes at the point of contact are parallel and align. The vectors $\mathbf{r}_1 - \mathbf{R}$ and $\mathbf{r}_2 - \mathbf{R}$ are normal to this plane and hence must be aligned. Thus we need only to define a single vector $\mathbf{C}_1$ to determine the locations of the two centrelines associated with s.

This fact allows us to define a single framing whose curvatures can be used to rebuild both rods (see Section 2.4). In this sense the birod structure can be seen as a Cosserat rod, discussed in section 2.1, with the vector fields $\mathbf{R}$ and $\mathbf{C}_1/||\mathbf{C}_1||$ playing the roles of $\mathbf{r}$ and $\mathbf{d}_1$, and the problem is to determine the mechanics of this composite rod.

In assuming that the cross-sections are always circular we imply that the length of the vector field $\mathbf{C}_1$ is constant. This also implies that we have restricted the cross-sections from deforming transversely, both assumptions are not always uniformly made in rope modelling (see e.g. [2]), and we briefly discuss the possibility of

relaxing these assumptions in Section 3.4. That said, unless the rods are significantly prone to such transverse deformations, our assumption does not seem unreasonable and significantly simplifies the following kinematic description of the individual rods, particularly in the cases where the curve $\mathbf{R}$ adopts a non-trivial (straight) configuration.

2.3 The Contact Frame

We define an orthonormal basis at the point of contact in order to describe the forces and moments acting there. In our case we define a moving framing $(\mathbf{D}_1, \mathbf{D}_2, \mathbf{D}_3)$ with unit vectors

$$\mathbf{D}_3 = \frac{\mathbf{R}'}{||\mathbf{R}'||}, \quad \mathbf{D}_1 = \frac{\mathbf{C}_1}{||\mathbf{C}_1||}, \quad \mathbf{D}_2 = \mathbf{D}_3 \times \mathbf{D}_1. \tag{10}$$

This frame is associated with a strain vector $\mathbf{U} = \mathsf{U}_1\mathbf{D}_1 + \mathsf{U}_2\mathbf{D}_2 + \mathsf{U}_3\mathbf{D}_3$ and spin vector $\mathbf{W} = \mathsf{W}_1\mathbf{D}_1 + \mathsf{W}_2\mathbf{D}_2 + \mathsf{W}_3\mathbf{D}_3$ such that $\mathbf{D}_i' = \mathbf{U} \times \mathbf{D}_i$ and $\dot{\mathbf{D}}_i = \mathbf{W} \times \mathbf{D}_i$. As with any rod frame, given $\mathbf{U}$ and $\mathbf{W}$ we can solve the system

$$\begin{pmatrix} \mathbf{D}_1' \\ \mathbf{D}_2' \\ \mathbf{D}_3' \end{pmatrix} = \begin{pmatrix} 0 & \mathsf{U}_3 & -\mathsf{U}_2 \\ -\mathsf{U}_3 & 0 & \mathsf{U}_1 \\ \mathsf{U}_2 & -\mathsf{U}_1 & 0 \end{pmatrix} \begin{pmatrix} \mathbf{D}_1 \\ \mathbf{D}_2 \\ \mathbf{D}_3 \end{pmatrix}, \quad \begin{pmatrix} \dot{\mathbf{D}}_1 \\ \dot{\mathbf{D}}_2 \\ \dot{\mathbf{D}}_3 \end{pmatrix} = \begin{pmatrix} 0 & \mathsf{W}_3 & -\mathsf{W}_2 \\ -\mathsf{W}_3 & 0 & \mathsf{W}_1 \\ \mathsf{W}_2 & -\mathsf{W}_1 & 0 \end{pmatrix} \begin{pmatrix} \mathbf{D}_1 \\ \mathbf{D}_2 \\ \mathbf{D}_3 \end{pmatrix}, \tag{11}$$

subject to the compatibility condition

$$\mathbf{W}' - \dot{\mathbf{U}} = \mathbf{U} \times \mathbf{W}, \tag{12}$$

to obtain the well-defined frame of the contact line at all t. Of interest in Sections 4-6 are straight-axis birod states characterised by functions $\mathsf{U}_1 = \mathsf{U}_2 = 0$, and a general function $\mathsf{U}_3 = \Phi'$ yielding the following rod centrelines

$$\mathbf{r}_1(s) = \begin{pmatrix} R\sin(\Phi(s) + c) \\ -R\cos(\Phi(s) + c) \\ s \end{pmatrix}, \quad \mathbf{r}_2 = (s) \begin{pmatrix} -R\sin(\Phi(s) + c) \\ R\cos(\Phi(s) + c) \\ s \end{pmatrix}. \tag{13}$$

If Φ' is constant this curve is a helix. A varying function Φ' yields a helix with varying pitch. In this particular case the parameter s is the arclength of the contact line.

2.4 Rod Geometry in the Contact Frame

Next we characterise the geometry of the two rods in terms of the geometry of the contact line. To do so we recast the rod kinematics in terms of the contact frame $\{\mathbf{D}_j\}$. The rods are defined by the function pairs $(\mathbf{r_1}, \mathbf{d}_{11})$ and $(\mathbf{r}_2, \mathbf{d}_{12})$, where we have used the notation $\mathbf{d}_{ji}$, with $j = 1, 2, 3$ labelling the particular vector of the basis of rod $i = 1, 2$ (*i.e.*, $\mathbf{d}_{32}$ is the tangent vector of rod 2).

The vectors $\mathbf{r}_i$ are defined by

$$\mathbf{r}_i(s,t) = \mathbf{R}(s,t) + (-)^{i+1} R\mathbf{D}_1(s,t). \tag{14}$$

with $R = ||\mathbf{C}_1||$ the (fixed) radius if the rods. Differentiating (14) w.r.t. s we have

$$\begin{aligned} \mathbf{r}_i' &= \mathbf{D}_3 + (-)^{i+1} R\mathbf{D}_1' \\ &= \left(1 + (-)^i R\mathsf{U}_2\right)\mathbf{D}_3 + (-)^{i+1} R\mathsf{U}_3\mathbf{D}_2. \end{aligned} \tag{15}$$

where we have used (11). In general this is not a unit vector. Indeed we have

$$\lambda_i^2 = \frac{\partial \mathbf{r}_i}{\partial s} \cdot \frac{\partial \mathbf{r}_i}{\partial s} = \frac{\partial \mathbf{r}_i}{\partial s_i} \cdot \frac{\partial \mathbf{r}_i}{\partial s_i} \left(\frac{\partial s_i}{\partial s}\right)^2 = \left(\frac{\partial s_i}{\partial s}\right)^2 = \left(1 + (-)^i R\mathsf{U}_2\right)^2 + R^2\mathsf{U}_3^2.$$

Hence,

$$\lambda_i(s,t) = \left(\left(1 + (-)^i R\mathsf{U}_2(s,t)\right)^2 + R^2\mathsf{U}_3(s,t)^2\right)^{1/2}. \tag{16}$$

The specific choice of parametrisation s places constraints on the functions λ_i. One possibility would be to choose s to be the arclength of rod 1, *i.e.*, $s_1 = s$. With this choice we would require $\lambda_1(s,t) = 1, \forall s, t$ and the integral constraint

$$\int_0^{L_1} \lambda_2(s,t)\ \mathrm{d}s = L_2,\ \forall t,$$

hold for the second rod. For a general parametrisation $s \in [s^{min}, s^{max}]$ we require the following two integral constraints are satisfied,

$$\int_{s^{min}}^{s^{max}} \lambda_1(s,t)\ \mathrm{d}s = L_1, \quad \int_{s^{min}}^{s^{max}} \lambda_2(s,t)\ \mathrm{d}s = L_2,\ \forall t. \tag{17}$$

Equations (4) and (6) give expressions for κ_i and τ_i of rod $\mathbf{r}_i$ in terms of the curvatures $(\mathsf{U}_1, \mathsf{U}_2, \mathsf{U}_3)$ and R, as functions of s. We define the pair $(\mathbf{d}_{1i}, \mathbf{d}_{2i})$ as

$$\begin{aligned} \mathbf{d}_{1i} &= \cos(\phi_i)\boldsymbol{\nu}_i + \sin(\phi_i)\boldsymbol{\beta}_i, \\ \mathbf{d}_{2i} &= -\sin(\phi_i)\boldsymbol{\nu}_i + \cos(\phi_i)\boldsymbol{\beta}_i, \end{aligned} \tag{18}$$

(see Figure 5(b)). It is important to remember that the functions ϕ_i are functions of s not s_i. With this labelling the form taken by the curvatures u_{ji} are

$$\mathsf{u}_{1i} = \kappa_i \sin(\phi_i), \quad \mathsf{u}_{2i} = \kappa_i \cos(\phi_i), \quad \mathsf{u}_{3i} = \frac{\phi_i'}{\lambda_i} + \tau_i. \tag{19}$$

The kinematics of the rods are completely defined in terms of the functions $(\mathsf{U}_1, \mathsf{U}_2, \mathsf{U}_3)$, the radius R, and the functions ϕ_i. The dynamics can be obtained from expressions for the time derivatives $\partial r/\partial s^n \partial t$ using (14) in conjunction with (11). Using (6) and (4) we can obtain time derivatives of the Frenet pairs $(\boldsymbol{\nu}_i, \boldsymbol{\beta}_i)$ and through (18) time derivatives $\dot{\mathbf{d}}_{1i}$ and $\dot{\mathbf{d}}_{2i}$. Using $\mathbf{d}_{3i} = \lambda_i \mathbf{r}_i'$ we can obtain the time derivatives $\dot{\mathbf{d}}_{3i}$ and through

$$\mathsf{w}_{1i} = \mathbf{d}_{3i} \cdot \dot{\mathbf{d}}_{2i}, \quad \mathsf{w}_{2i} = -\mathbf{d}_{3i} \cdot \dot{\mathbf{d}}_{1i}, \quad \mathsf{w}_3 = \mathbf{d}_{2i} \cdot \dot{\mathbf{d}}_{1i}. \tag{20}$$

the components of the spin vectors $\mathbf{w}_{ji}$ for each rod.

Finally, it is necessary to show that the individual compatibility conditions of the two rods are satisfied if (12) is satisfied. Indeed we can write the arclength derivative $\mathbf{r}_i'$ as a linear combination of the basis $(\mathbf{D}_1, \mathbf{D}_2, \mathbf{D}_3)$ through (15). If (12) is satisfied then the vector fields $\mathbf{D}_j$ have commuting partial derivatives, so the vectors $\mathbf{r}_i'$ must also have commuting partial derivatives, as must $\mathbf{d}_{3i} = \lambda_i \mathbf{r}'$. The same is also true of any further s partial derivatives of $\mathbf{r}_i$ as they are always linear combinations of the basis $(\mathbf{D}_1, \mathbf{D}_2, \mathbf{D}_3)$. With this we can conclude from (4) that the vectors $(\boldsymbol{\nu}_i, \boldsymbol{\beta}_i)$ satisfy.

$$\frac{\partial \boldsymbol{\nu}}{\partial s \partial t} = \frac{\partial \boldsymbol{\nu}}{\partial t \partial s}, \text{ and } \frac{\partial \boldsymbol{\beta}}{\partial s \partial t} = \frac{\partial \boldsymbol{\beta}}{\partial t \partial s}, \tag{21}$$

and from (18) so do the linear combinations $\mathbf{d}_{1i}$ and $\mathbf{d}_{2i}$. Finally, as we have shown all of $\mathbf{d}_{ji},\ j = 1,2,3,\ i = 1,2$ have commuting partial derivatives, the individual rod compatibility conditions will automatically be satisfied.

3 Mechanics

We couple the balance equations of the individual rods with their interaction at the contact line. These equations were originally derived in [26] independent of the strict contact line kinematics the authors then enforced. They are

$$\mathbf{n}_i' + \mathbf{F}_i + \mathbf{f}_i = \rho \ddot{\mathbf{r}}_i, \tag{22}$$

$$\mathbf{m}_i' + \mathbf{r}_i' \times \mathbf{n}_i + (-1)^i R \mathbf{D}_1 \times \mathbf{F_i} + \mathbf{L}_i + \mathbf{l}_i = \rho I \left(\mathbf{d}_{1i} \times \ddot{\mathbf{d}}_{1i} + \mathbf{d}_{2i} \times \ddot{\mathbf{d}}_{2i} \right), \tag{23}$$

$$\mathbf{F}_1 = -\mathbf{F}_2, \tag{24}$$

$$\mathbf{L}_1 = -\mathbf{L}_2. \tag{25}$$

With ρ the density of the rods (assumed to be the same) and I the second moment of inertia of the bodies, which for circular cross-sections is $\pi R^4/4$. The fields $\mathbf{n}$ and $\mathbf{m}$ are the force and moment respectively acting across a cross-section of the rod. The vector field $\mathbf{F}$ represents a body force per unit contact length due to contact. In this case $\mathbf{F}_1$ represents the force exerted on rod 1 by rod 2. This force vanishes when there is a loss of contact.

Equations (22) represent the internal balance of linear momentum in the rod and the forces $\mathbf{f}_i$ represent any other body forces acting at the rod centrelines. Equations (23) represent the balance of angular momentum in the individual rods. The contact force $\mathbf{F}_i$ produces a moment in (23) as it is applied at the contact line on the rod's surface. The body moment $\mathbf{L}_1$ is the contact moment per unit length of $\mathbf{R}$ imposed on $\mathbf{r}_1$ by rod $\mathbf{r}_2$, acting at the contact line, and similar for $\mathbf{L}_2$. The couples $\mathbf{l}_i$ represent any other body couples acting at the rod centrelines. Finally (24) and (25) are Newton's third law at the line of contact.

For unstretchable-unsherable Cosserat rods a constitutive moment is supplied to complete the individual rod equations by specifying functions m_{ji} of the form

$$\mathsf{m}_{ji} = \mathsf{m}_{ji}(\mathsf{u}_{j1}, \mathsf{u}_{j2}, \mathsf{u}_{j3}, s_i).$$

We have shown how to re-write any such kinematic relationship in terms of the contact curvatures U_i, the functions ϕ_i and the contact parameter s (the curvatures U_i are also invariant to the group of Euclidean transformations [26]). Our birod model is applicable given any suitable choice of constitutive relationship (see *e.g.*, Antman Chapter 8 [1]). In sections 4-6 we derive an approximate linear constitutive law for a birod by assigning the rods the linear constitutive relationship of a transversely isotopic rod whose reference state (with zero applied forces and moments) is straight. In dimensionless form this is

$$\mathbf{m}_i = \kappa_i \sin(\phi_i)\mathbf{d}_{1i} + \kappa_i \cos(\phi_i)\mathbf{d}_{2i} + \gamma\left(\tau_i + \frac{\phi_i'}{\lambda_i}\right)\mathbf{d}_{3i}. \tag{26}$$

see [18] for details of the appropriate length/time/mass scalings. The dimensionless constant γ is the ratio of the twisting moment of inertia to the bending moment of inertia, its takes values on the domain $\gamma \in [\frac{2}{3}, 1]$, with 1 corresponding to a hyper-elastic material and 2/3 an incompressible material. The choice (26) is generally referred to as the Kirchhoff rod model and assumes the dimensionless quantity

$$\max_{\forall s,t}\left\{\sqrt{\mathsf{u}_{1i}^2 + \mathsf{u}_{2i}^2 + \mathsf{u}_{3i}^2}R, \frac{R}{L_i}\right\}, \tag{27}$$

is small [17]. In solving the equations we will use equations (4), (18) and (6) to express the moments $\mathbf{m}_i$ in terms of the contact basis. Whatever the choice of constitutive law for $\mathbf{m}$, the forces $\mathbf{n}_i$ are expressed directly in the contact basis

$$\mathbf{n}_i = \mathsf{n}_{1i}\mathbf{D}_1 + \mathsf{n}_{2i}\mathbf{D}_2 + \mathsf{n}_{3i}\mathbf{D}_3, \tag{28}$$

Note we do not denote the components of the vectors $\mathbf{n}_i$ in capitals, even though they are expressed in the contact basis, as they are forces acting at the rod centrelines **not** the contact line.

3.1 Composite Mechanics of the Birod

The net force acting at $\mathbf{R}(s)$ is

$$\mathbf{N} = \mathbf{n}_1 + \mathbf{n}_2. \tag{29}$$

The net moment acting about the contact line $\mathbf{R}(s)$ is,

$$\mathbf{M} = \mathbf{m}_1 + \mathbf{m}_2 + R\mathbf{D}_1 \times \mathbf{N}_d, \quad \mathbf{N}_d = \mathbf{n}_1 - \mathbf{n}_2. \tag{30}$$

3.2 Solving the System

Taking into account (24) and (25) there are 32 unknowns $(\mathbf{n}_1, \mathbf{n}_2, \mathbf{F}, \mathbf{L}, \mathbf{f}_1, \mathbf{f}_2, \mathbf{l}_1, \mathbf{l}_2, \mathsf{U}_1, \mathsf{U}_2, \mathsf{U}_3, \mathsf{W}_1, \mathsf{W}_2, \mathsf{W}_3, \phi_1, \phi_2)$ and 15 equations from (22), (23) and the compatibility constraints (12). If we assume body forces/moments have been specified using constitutive laws, additional equations, or are absent, we are still five equations short of a complete system. Of course this imbalance can also be removed by specifying constitutive laws for five of the components of $\mathbf{F}$ and $\mathbf{L}$, as we shall discuss. Alternatively there are five independent degrees of freedom of rod geometry, relative to the contact basis, on which geometric constraints can be applied in order to complete the system.

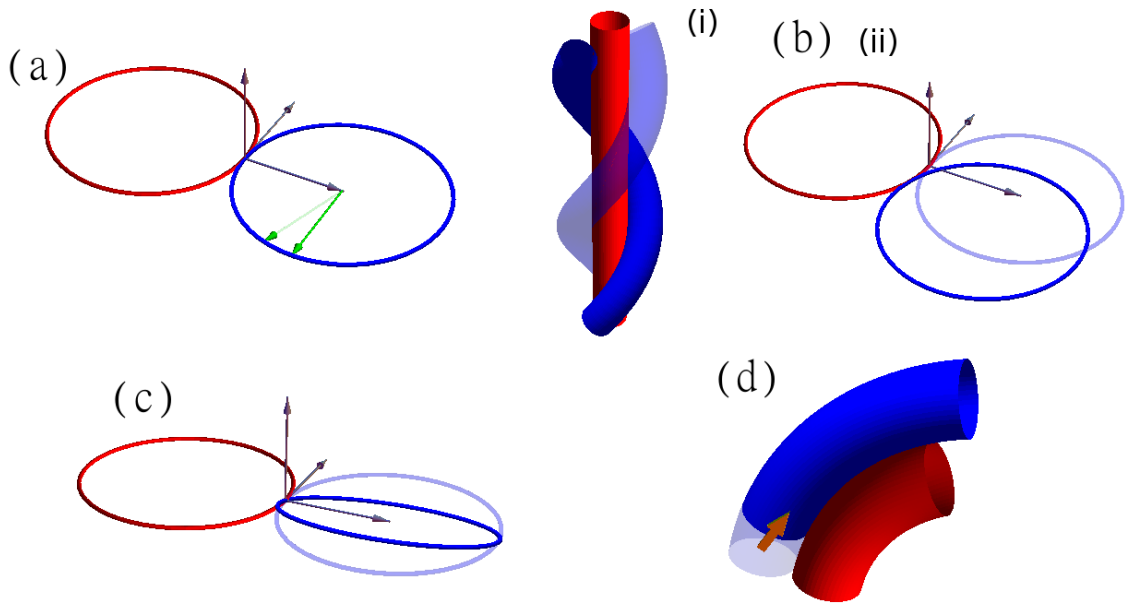

Fig. 6 Figures depicting the relative motions of the birod which may lead to contact forces/moments. Panel (a) represents the internal twisting of the rod. Panel (b)(i) depicts the wrapping of one rod about the other (the translucent disc is its original position), leading into a change of point of contact of the two discs as shown in (b)(ii). Panel (c) represents a screwing motion which would be associated with changes in curvature of the rods. Panel (d) depicts the sliding of the two rods past each other

3.2.1 Relative Rod Geometry

Firstly the vector $\mathbf{D}_1$ can be written as a linear combination of the pairs $(\mathbf{d}_{1i}, \mathbf{d}_{2i})$ spanning the rod cross-sections,

$$\mathbf{D}_1 = \cos(\alpha_1)\mathbf{d}_{11} + \sin(\alpha_1)\mathbf{d}_{21} = \cos(\alpha_2)\mathbf{d}_{12} + \sin(\alpha_2)\mathbf{d}_{22}. \tag{31}$$

The angles α_i will in part result from the internal rotation of the material discs composing the rod, as characterised by the twist functions u_{3i} (Figure 6(a)), but also motions due to the relative rotation of two rods, as depicted in Figure 6(b)(i)-(ii).

Secondly the vectors $\mathbf{d}_{3i}$ are perpendicular to $\mathbf{D}_1$ and must be representable as a linear combination of the pair $(\mathbf{D}_2, \mathbf{D}_3)$,

$$\mathbf{d}_{31} = \cos(\beta_1)\mathbf{D}_3 + \sin(\beta_1)\mathbf{D}_2, \quad \mathbf{d}_{32} = \cos(\beta_2)\mathbf{D}_3 + \sin(\beta_2)\mathbf{D}_2. \tag{32}$$

The angles β_i can be used to quantify the screwing motion depicted in (Figure 6(c)). As an example for helical birods $\beta_1 = -\beta_2$ and both are constant with respect to s. In this case β is equal to the helical angle made by $\mathbf{d}_3$ and $\hat{\mathbf{z}}$. Increasing/decreasing β corresponds to an increasing/decreasing helical pitch.

The final degree of freedom concerns relative sliding motions of the two rods along the contact line (Figure 6(d)). To quantify this effect we must first define a reference configuration with parametrisation $s_r \in [s_r^{min}, s_r^{max}]$ for which we can assign functions $s_1^r(s_r)$ and $s_2^r(s_r)$, specifying the arclengths of points on the rod axes $\mathbf{r}_1$ and $\mathbf{r}_2$ whose material discs are in contact in this reference configuration. The sliding can then be defined for all admissible configurations by defining a function $\Delta s(s_r)$, which specifies the separation, in terms of the reference contact parameter s_r, of the two points which were initially contacting. Using the integral relationships

$$s_1(s_r, t) = \int_{s_r^{min}}^{s_r} \lambda_1(s, t)\ \mathrm{d}s, \quad s_2(s) = \int_{s_r^{min}}^{s_r} \lambda_2(s, t)\ \mathrm{d}s, \tag{33}$$

the function Δs is given by the sum

$$\Delta s(s_r, t) = (s_1(s_r, t) - s_1^r(s_r)) + (s_2(s_r, t) - s_2^r(s_r)). \tag{34}$$

The choice $\Delta s = 0, \forall s_r, t$ corresponds to forbidding sliding motions.

3.2.2 Completing the System - Geometric Constraints

The most straight-forward example of geometric constraints would be what we refer to as the "*perfect glue*" corresponding to fixing the rod geometry with respect to the contact frame for all admissible configurations. We denote $\mathcal{P}_0$ as the set of initial birod variables $\mathcal{P}_0 = \left\{\mathbf{n}_1^{(0)}, \mathbf{n}_2^{(0)}, \mathbf{F}^{(0)}, \mathbf{L}^{(0)}, \mathsf{U}_1^{(0)}, \mathsf{U}_2^{(0)}, \mathsf{U}_3^{(0)}, \mathsf{W}_1^{(0)}, \mathsf{W}_2^{(0)}, \mathsf{W}_3^{(0)}, \phi_1^{(0)}, \phi_2^{(0)}\right\}$, and some other admissible set of these variables $\mathcal{P}$. We define the functional Δf, for some function f dependent on the parameter sets $\left\{\mathcal{P}, \mathcal{P}^0, s\right\}$, as

$$\Delta f(\mathcal{P}, \mathcal{P}^0, s) = f(\mathcal{P}, \mathcal{P}_0, s) - f(\mathcal{P}_0, s), \tag{35}$$

and the perfect glue would require the following hold for all s

$$\begin{aligned} \Delta\alpha_1(\mathcal{P}, \mathcal{P}_0, s) = 0, \quad \Delta\alpha_2(\mathcal{P}, \mathcal{P}_0, s) = 0, \\ \Delta\beta_1(\mathcal{P}, \mathcal{P}_0, s) = 0, \quad \Delta\beta_2(\mathcal{P}, \mathcal{P}_0, s) = 0, \\ \Delta s(\mathcal{P}, \mathcal{P}_0, s) = 0, \end{aligned}$$

for for all admissible configurations. More generally we require a system of equations $\mathcal{C}_k$, such that

$$\mathcal{C}_k\left(\alpha_1, \alpha_2, \beta_1, \beta_2, \Delta s, \mathcal{P}, \mathcal{P}_0, s\right) = 0, \quad k = 1, 2, 3, 4, 5,$$

The solutions of the system comprising these equations, (22)-(25) and (12) will determine the functions $\Delta\alpha_i, \Delta\beta_i, \Delta s$ (subject to the application of boundary conditions).

3.2.3 Constitutive Laws

Alternatively we can provide constitutive laws for the contact moments through equations G_k, that is

$$\begin{aligned} \mathsf{F}_2 = G_1(\mathcal{P}_0, \mathcal{P}, s), \quad \mathsf{F}_3 = G_2(\mathcal{P}_0, \mathcal{P}, s), \\ \mathsf{L}_1 = G_3(\mathcal{P}_0, \mathcal{P}, s), \quad \mathsf{L}_2 = G_4(\mathcal{P}_0, \mathcal{P}, s), \quad \mathsf{L}_3 = G_5(\mathcal{P}_0, \mathcal{P}, s). \end{aligned} \tag{36}$$

with F_1, the mutual pressure which is exerted by the rods on each other, determined by solving the system (22)-(25) and (12) with the laws (36) inserted. Solving the complete system will determine the functions $\Delta\alpha_i, \Delta\beta_i, \Delta s$.

A particular case of applying force/moment constraints which has been treated in the literature on several occasions is to set all the functions $G_k = 0, \forall s \in (s^{min}, s^{max})$ (*i.e.*, on the birod's interior) [44,43,29,47,41]. This assumes the other contact force/moments restricting sliding/twisting motions are negligible by comparison to the normal contact pressure F_1. For well-lubricated wire ropes and weakly bonded coiled-coil structures this assumption is probably valid. It is this choice which we make in Sections 4-6. In this case we require alternative and far more restrictive constraints on the boundary in order to keep the structure self-contacting, we use geometric constraints in Sections 4-6.

3.3 Boundary Geometric Constraints

By applying only a set $(N_1, N_2, N_3, M_1, M_2, M_3)$ at a boundary we would appear to be six short of the number of required constants required to specify the set $\mathbf{m}_1, \mathbf{m}_2, \mathbf{n}_1, \mathbf{n}_2$. However, the 6 moments functions $\mathsf{m}_i, i = 1, 2$, are actually functions of 5 kinematic variables $(\mathsf{U}_1, \mathsf{U}_2, \mathsf{U}_3, \phi_1, \phi_2)$. So by providing 5 rules which constrain the set $(\Delta\alpha_1, \Delta\alpha_2, \Delta\beta_1, \Delta\beta_2, \Delta s)$ at the boundaries we can remove this ill-definition.

We denote the upper and lower boundary s-values B^+ and B^-. Firstly have demanded that the rods are in contact for their whole lengths so the end points of the two rods must always coincide, *i.e.*, $\Delta s(B^{\pm}) = 0$ for all admissible deformations. Secondly, upon solving the balance equations on the birod's interior $s \in (B^-, B^+)$ it will be possible to specify the angles α_i and β_i in terms of the applied force/moments $M_1^{\pm}, M_2^{\pm}, M_3^{\pm}, N_1^{\pm}, N_2^{\pm}, N_3^{\pm}$ and the rod lengths (L_1, L_2) (required to apply the boundary conditions in conjunction with the length constraints

(17)). We refer to this parameter set as $\mathcal{P}^b$,and have the set $\mathcal{P}_0^b$ be the case in which all forces and moments are zero. The boundary constraints for the perfect glue we have discussed above would be

$$\begin{aligned} \Delta\alpha_1(\mathcal{P}^b, \mathcal{P}_0^b, B^\pm) &= 0, \\ \Delta\alpha_2(\mathcal{P}^b, \mathcal{P}_0^b, B^\pm) &= 0, \\ \Delta\beta_1(\mathcal{P}^b, \mathcal{P}_0^b, B^\pm) &= 0, \\ \Delta\beta_2(\mathcal{P}^b, \mathcal{P}_0^b, B^\pm) &= 0, \\ \Delta s(\mathcal{P}^b, \mathcal{P}_0^b, B^\pm) &= 0, \end{aligned} \tag{37}$$

for all admissible configurations.

3.3.1 Helical Birods

In general we may not require such rigid conditions. For example it was demonstrated in [29] that it is possible to gradually tighten a helical birod under the action of an applied load and moment, such that its remains uniformly helical and satisfies the birod equilibrium equations. This would not be possible under the set of conditions (37) as it requires the angles β_1 and β_2 change when the vectors $\mathbf{d}_{3i}$ of (13) rotate about $\mathbf{N}_1$ to obtain a lower pitch. In fact it was shown in using variational analysis of a straight axis birod in [47] that the required boundary constraints for this uniform tightening would be

$$\Delta\frac{\partial\beta_i}{\partial s}(\mathcal{P}^b, \mathcal{P}_0^b, B^\pm) = 0. \tag{38}$$

for all admissible equilibrium configurations. (*c.f.* [47] $\theta = \beta_1 = -\beta_2$, $\psi = \mathsf{u}_3$ and the same symbol is used for ϕ) and, as shown in Section A of the Appendix, the equivalent conditions on the angles α_i would be either

$$\Delta\alpha_i(\mathcal{P}^b, \mathcal{P}_0^b, B^\pm) = 0, \text{ or } \Delta\frac{\partial\alpha_i}{\partial s}(\mathcal{P}^b, \mathcal{P}_0^b, B^\pm) = 0. \tag{39}$$

for all admissible configurations.

3.3.2 Sufficiently Pinned Conditions

In sections 4-6 we do not consider specific boundary constraints, rather we restrict the motion of the individual rods with respect to the contact frame at the boundaries, such that the change in the angles (α_i, β_i) with changing shape of the birod are bounded,

$$\begin{aligned} |\Delta\alpha_1(\mathcal{P}^b, \mathcal{P}_0^b, B^\pm)| &\leq \alpha_{1m}, \\ |\Delta\alpha_2(\mathcal{P}^b, \mathcal{P}_0^b, B^\pm)| &\leq \alpha_{2m}, \\ |\Delta\beta_1(\mathcal{P}^b, \mathcal{P}_0^b, B^\pm)| &\leq \beta_{1m}, \\ |\Delta\beta_2(\mathcal{P}^b, \mathcal{P}_0^b, B^\pm)| &\leq \beta_{2m}, \\ \Delta s(\mathcal{P}^b, \mathcal{P}_0^b, B^\pm) &= 0 \end{aligned} \tag{40}$$

If the upper bounds α_{im}, β_{im} are small this corresponds to boundary laws **similar** to the perfect glue (37), in that they restrict the motion of the individual rods relative to the contact basis on the boundary. We show in Section (6) that if the upper bounds are small with respect to the length L of the birod and of the same order (or smaller) as its radius R then the birod's averaged mechanical response is independent of the particular choice of boundary constraints, assuming the individual rods have the dimensions required by the Kirchhoff model.

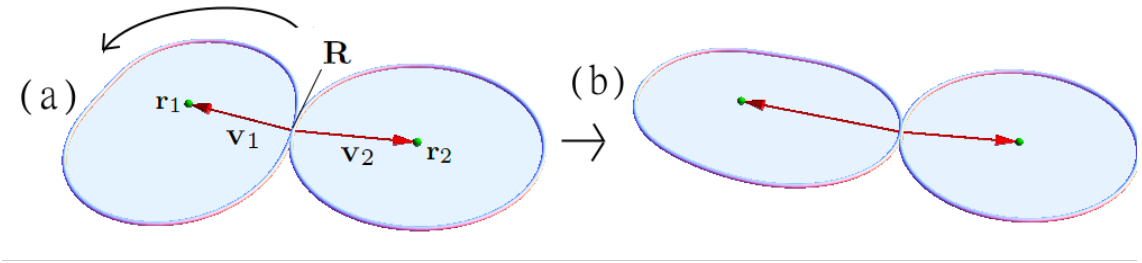

Fig. 7 Depictions of non-circular cross sections. Panel (a) depicts a convex, non-circular, cross-section. The vectors $\mathbf{v}_1$ and $\mathbf{v}_2$ joining $\mathbf{R}$ to the curves $\mathbf{r}_1$ and $\mathbf{r}_2$ are shown. Panel (b) depicts the consequence of rotating the rod $\mathbf{r}_1$, we see the vector $\mathbf{v}_1$ is now significantly longer than it was in panel (a).

3.4 Relaxing Various Model Assumptions

The model makes a number of assumptions regarding the birod's kinematics, namely:

1. Circular cross-sections
2. Continual contact of the rods
3. The number of rods composing the structure

We briefly discuss the possibility of relaxing these constraints as an insight to possible elaborations on the birod model. It is impossible to conduct an exhaustive discussion of these issues here so we keep the discussion brief. What follows is **not** required for Sections 4-6.

Rods with convex cross-sections can form a birod structure. Their surface tangent spaces must still be parallel at contact so we can define the vector $\mathbf{C}_1$ as in Section 2.3, and hence the contact frame $\{\mathbf{D}_i\}$. The point $\mathbf{r}_i(s)$ can then be written in the form $\mathbf{R}+\mathbf{v}_i$, with $\mathbf{v}_i$ some linear combination of the frame vectors $\{\mathbf{D}_i\}$ (see Figure 7(a)). With this assumption equations (14)-(16) would need to altered, but equations (17)-(20), in conjunction with (4) and (6), can still be used to define the curvatures u_{ij} of the individual rods. Additionally equations (31) and (32), (33) and (34) would still apply, so we can completely define the kinematic description of the rods in terms of the contact line $\mathbf{R}$, the angles β_i and α_i, and the function Δ_s. However, the description could be heavily dependent on the potential deformation of the rod. For example rotation of non circular cross-sections would cause the distance of the point $\mathbf{r}(s)$ to the line of contact to change as in Figure 7(b). So the equation $\mathbf{r}_i = \mathbf{v}_i+\mathbf{R}$ could depend on the parameters α, β and Δ_s, whilst the circular cross-section relations $\mathbf{r}_i = \mathbf{R}+R\mathbf{D}_1$ do not.

We could also include the possibility of transverse deformations of the cross-sections under the mutual applied pressure F_1. This possibility and its affect on the pressure is considered by Argatov [2], who treats the local contact problem using matched asymptotic expansions and uses this result to modify the pressure obtained by solving the equilibrium equations of helical rope model composed of Kirchhoff rods.

If the rods loose contact for some sub-section of their length then the mechanical equations must decouple and the forces/couple pair $(\mathbf{F},\mathbf{L})$ vanish. Similarly the rod kinematics would also decouple. It would be sensible to treat the rods individually on non-contacting domains and as birods on the domain of mutual contact; unless specific assumptions could be made of the individual rod geometries on the non-contacting s-domain. Part of the problem would then be to determine the size of each domain. One must also consider the continuity of the balance equations at the point where contact is lost/retained, Coleman and Swigon [9] detail this condition explicitly for the self-contact of an individual rod and the same considerations would apply for the contact of two different rods.

Rather than contacting rods, one might consider two rods which are connected by some set of rigid vectors. For example this could mimic the strong covalent bonds holding a DNA molecule together. The centre of these vectors would play the role of the curve $\mathbf{R}$ and the joining vectors the role of the vectors $\mathbf{C}_1$ and $\mathbf{C}_2$. The kinematic expressions of Sections 2.2 and 2.4 would then be applicable, though the distance R would no longer play the role of the rod radii. As the rods are no longer contacting the forces acting on the rod surfaces $(\mathbf{F}_i,\mathbf{L}_i)$ do not necessarily have to satisfy (24) and (25). Instead they would need to be determined by the manner in which the joining vectors interact with the rods and/or some appropriate long-range interaction laws.

Neukirch and van der Heijden [29] considered n inter-twined helical rods surrounding and empty core and Morimoto and Iizuka [27] extended this work to include a compressible filled core. One could further extend the work of [27] to consider more general geometries of the central curve of the system, which is the centre of the filled core. This curve would play the role of the contact line $\mathbf{R}$ and the geometry of the individual rods could be expressed as functions of the curvature of $\mathbf{R}$. The system would then have n rod equations of the form (22) and (23) and a requisite number of interaction couplings of the form (24) and (25). For example a rod contacts two others in [29] and three, core included, in [27]. There would be significant difficulties from a kinematic standpoint. First, one must apply the conditions of non-overlapping contact for each pair of rods as a set of additional constraint (see [9,29]). This is not necessary in the case of two rods, where there mutual non-overlapping contact can be assured by assuming the vector $\mathbf{C}_1$ is normal to the tangent vector of the contact line (see Section 2.2). Second, the relative degrees of freedom of two contacting rods discussed in Section 3.2.1 would have to be described in a local basis different form the centreline centre line basis $\mathbf{R}$.

4 Determining the Linear Response of a Helical Birod

We consider a birod in the absence of any additional body forces $\mathbf{f}_i = 0$, $\mathbf{l}_i = 0$, $i = 1, 2$. The birod's interaction mechanics are specified on the interior through constitutive laws (36) with $G_k = 0$, $k = 1, 2, 3, 4, 5$, so that the only possible interaction force is the normal pressure F_1. This is exactly the choice made in the equilibrium study of birod structures by Starostin and van Der Heijden [41]. We consider rods of equal length L_r and demand the boundary laws discussed in Section (3.3) satisfy the constraints (40). We assume the individual rods obey the linear constitutive law (26), for which the rods are naturally straight in the absence of applied force/moment combinations.

We define a "straight" birod to be a helical birod of the form (13), with $\Phi'(s)$ having a constant value. In this reference state the parameter s is the arclength of the birod. It was shown in [43,29,47] that this birod configuration has equilibrium solutions with $\mathbf{N} = \mathbf{M} = 0, \forall s$, we briefly re-derive this results here as we use a different parametrisation and basis. In section 5 we then compute a expansion of the contact frame about this state to linear order, solve the linearised system (22)-(25) assuming it is in equilibrium, and compare the corrected frame curvatures to the net applied forces and moments to establish the linear response of the birod.

The parametrisation of the deformed configurations is the arclength of the contact line in the given configuration. In general this would be a rather odd choice to make as the contact line's length is not fixed for all admissible configurations. However, the particular linearisation procedure we use is such that the correction to arclength is of quadratic order and at linear order the change in length of the contact line must be enforced using the identities (17), in this case the limits (s^{min}, s^{max}) will change as well as the functions λ_i.

The birod's constituent rods have zero reference twist and for our effective birod to match this we must define a new untwisted contact line framing.

4.1 The Effective Rod Frame

By applying an appropriate counter rotation though Φ to the contact basis we obtain a basis $\mathbf{D}_{1r}, \mathbf{D}_{2r}, \mathbf{D}_3$ which is untwisted in the initial helical state (48), where

$$\mathbf{D}_{1r} = \mathbf{D}_1 \cos(\Phi) - \mathbf{D}_2 \sin(\Phi), \tag{41}$$
$$\mathbf{D}_{2r} = \mathbf{D}_1 \sin(\Phi) + \mathbf{D}_2 \cos(\Phi) \tag{42}$$

The effective rod curvatures for deformed configurations can be obtained by differentiating (41) and (42) to obtain curvatures $(\mathsf{U}_{1r}, \mathsf{U}_{2r}, \mathsf{U}_{3r})$ with

$$\mathsf{U}_{1r} = \mathsf{U}_1 \cos(\Phi) - \mathsf{U}_2 \sin(\Phi), \tag{43}$$
$$\mathsf{U}_{2r} = \mathsf{U}_1 \sin(\Phi) + \mathsf{U}_2 \cos(\Phi), \tag{44}$$
$$\mathsf{U}_{3r} = \mathsf{U}_3 - \Phi'. \tag{45}$$

Similarly the force components of $\mathbf{N}_r$ and $\mathbf{M}_r$ are

$$\mathsf{N}_{1r} = \cos(\nu_0 s)\mathsf{N}_1 - \sin(\nu_0 s)\mathsf{N}_2, \quad \mathsf{N}_{2r} = \sin(\nu_0 s)\mathsf{N}_1 + \cos(\nu_0 s)\mathsf{N}_2 \tag{46}$$

$$\mathsf{M}_{1r} = \cos(\nu_0 s)\mathsf{M}_1 - \sin(\nu_0 s)\mathsf{M}_2, \quad \mathsf{M}_{2r} = \sin(\nu_0 s)\mathsf{M}_1 + \cos(\nu_0 s)\mathsf{M}_2,$$

$$\mathsf{N}_{r3} = \mathsf{N}_3, \quad \mathsf{M}_{r3} = \mathsf{M}_3. \tag{47}$$

We solve the balance equations in the birod frame $(\mathbf{D}_1, \mathbf{D}_2, \mathbf{D}_3)$, however, for the purpose of determining a linear constitutive relationship for the birod we compare the linear corrections of U_{ir} to the forces $\mathbf{N}_{ir}$ and moments $\mathbf{M}_{ir}$ to determine the linear response of the effective birod.

4.2 The Zeroth Order

A good way to characterise a helical structure is by its helical angle θ, the constant angle made by the tangent vector of the helix and the $\hat{\mathbf{z}}$ direction. In terms of θ and R, the radius of the helix, the two rod centrelines can be written as

$$\mathbf{r}_1 = \begin{pmatrix} R\sin(\psi_1(s_1)) \\ -R\cos(\psi_1(s_1)) \\ s_1\cos(\theta) \end{pmatrix}, \quad \mathbf{r}_2 = \begin{pmatrix} -R\sin(\psi_2(s_2)) \\ R\cos(\psi_2(s_2)) \\ s_2\cos(\theta) \end{pmatrix}, \quad \psi_i = \frac{\sin(\theta)s_i}{R}. \tag{48}$$

the arclength functions are equal $s_1 = s_2$, and hence $\psi_1 = \psi_2$. The contact line is clearly a straight line

$$\mathbf{R}(s) = \begin{pmatrix} 0 \\ 0 \\ s_1\cos(\theta) \end{pmatrix}$$

A positive θ value gives a right-handed helical pair, $\theta < 0$ left-handed. By comparison to (13) we have the relationship $s = s_1\cos(\theta)$, *i.e.*, $\lambda_1 = \sec(\theta)$. Also $\mathsf{U}_1 = \mathsf{U}_3 = 0$ and $\mathsf{U}_3 = \Phi' = \tan(\theta)/R$ from substituting for s in the functions ψ_i. It was shown in [29] that if $|\theta| < \pi/4$ then the two rods must necessarily be overlapping and we must only consider the domain $\theta \in (-\pi/4, \pi/4)$. The curvature and torsion of $\mathbf{r}_1$ and $\mathbf{r}_2$ are equal, constant, and given by

$$\kappa = \frac{\sin^2(\theta)}{R}, \quad \tau = \frac{\sin(\theta)\cos(\theta)}{R}. \tag{49}$$

Substituting (48) and $s = s_1\cos(\theta) = s_2\cos(\theta)$ into (4) and then (18) we have the following expressions for the director basis

$$\mathbf{d}_{1i} = (-1)^i\cos(\phi_i(s))\mathbf{D}_1 + \sin(\phi_i(s))((-1)^i\cos(\theta)\mathbf{D}_2 + \sin(\theta)\mathbf{D}_3), \tag{50}$$

$$\mathbf{d}_{2i} = (-1)^{i+1}\sin(\phi_i(s))\mathbf{D}_1 + \cos(\phi_i(s))((-1)^i\cos(\theta)\mathbf{D}_2 + \sin(\theta)\mathbf{D}_3), \tag{51}$$

$$\mathbf{d}_{3i} = (-1)^{i+1}\sin(\theta)\mathbf{D}_2 + \cos(\theta)\mathbf{D}_3. \tag{52}$$

In the Appendix Section B the system (22)-(25) is solved for this helical state. The functions ϕ_i are linear and we write $\phi_i' = \phi_i^{(0)}$, the contact pressure F_1 is constant. The effective rod force has only a $\mathbf{D}_3$ component

$$\mathbf{N} = \left(\frac{2R^3\mathsf{F}_1\cot^2(\theta) + \sin(\theta)\cos(\theta)(2(\gamma-1)\sin(\theta) + \gamma R(\omega_1+\omega_2))}{R^2}\right)\mathbf{D}_3 \tag{53}$$

also the force difference is

$$\mathbf{N}_d = 2R\mathsf{F}_1\cot(\theta)\mathbf{D}_2 + \frac{\gamma\sin(\theta)\cos(\theta)(\omega_1-\omega_2)}{R}\mathbf{D}_3, \tag{54}$$

and the total rod moment also has only an $\mathbf{D}_3$ component

$$\mathbf{M} = \frac{2R^3\mathsf{F}_1\cot(\theta) + 2\sin^3(\theta) + \gamma\cos^2(\theta)(2\sin(\theta) + R(\omega_1-\omega_2))}{R}\mathbf{D}_3. \tag{55}$$

As $\mathbf{N}$ and $\mathbf{M}$ have only $\mathbf{N}_3$ components they are the same as $\mathbf{N}_r$ and $\mathbf{M}_r$. There are three constants to be determined by the boundary conditions, the two rates ω_1, ω_2 and the mutual pressure F_1 exerted by the rods

on each other. For this study it seems reasonable to assume that $\omega_1 = \omega_2 = \omega$. The total force has a constant value N_{3r}, applying this to (53) we have

$$\mathsf{F}_1 = \frac{\tan(\theta)\left(\mathsf{N}_{3r}\tan(\theta) - \frac{\sin^2(\theta)((\gamma-1)\sin(\theta)+\gamma R\omega)}{R^2}\right)}{R} \tag{56}$$

The total moment also has a constant value M_{3r}, then substituting (56) into (55) we obtain

$$\omega = \frac{\sec(2\theta)(R(\mathsf{M}_{3r} - \mathsf{N}_{3r}R\tan(\theta)) - 2\sin(\theta)((\gamma-1)\cos(2\theta)+1))}{2\gamma R}. \tag{57}$$

and the $\mathbf{D}_3$ component of $\mathbf{N}_d$ would vanish. It can be checked that by multiplying (57) by $\cos(\theta)$ the factor relating the rod arclengths to the contact line arclength we can then obtain equation (47) of [29].

Our effective zeroth order is one for which $\mathsf{M}_{3r} = \mathsf{N}_{3r} = 0$, with this we have

$$\mathsf{F}_1 = \frac{4\sin^5(\theta)\csc(4\theta)}{R^3}, \quad \omega = -\frac{\sin(\theta)(\gamma + \sec(2\theta) - 1)}{\gamma R}. \tag{58}$$

For this birod we have

$$\alpha_1(s) - \pi = \alpha_2(s) = -\omega s - c, \tag{59}$$

$$\beta_1(s) = -\beta_1(s) = \theta. \tag{60}$$

Which are obtained by comparing equations (50) and (51) to (31) and (52) to (32).

4.3 A Word on Boundary Conditions

This solution requires the specific boundary constraints that $\beta_1' = \beta_2' = 0$. We could have created such a uniformly helical birod from two aligned straight rods by gradually increasing the value of Φ under the boundary constraints discussed in Section 3.3.1. A more obvious means of creating such a helical configuration was detailed in [29]. Two initially straight rods were subjected to a fixed input twist, glued together at their ends, and then allowed to relax creating apparently helical configurations. Mathematically this could be enforced by the restrictive conditions (37). The authors observed in [47] that these conditions lead to a boundary layer of helical tightening of the birod at its ends (characterised by a changing rate of Φ), but a fixed value for the majority of the interior (the kind of behaviour shown in Figure 9(b)). In this case our model will be assumed to apply to this uniform section. However the uniformly helical section of birod has been created, we now assume it is subjected to an applied force and moment pair $(\mathbf{N}, \mathbf{M})$, under some boundary constraints which satisfy the sufficiently pinned conditions (40).

4.4 A Word on the Divergence of the Birod Forces

From (53) and (54) (with $\omega_1 = \omega_2$) it is always necessary to apply equal and opposite forces along the direction $\mathbf{D}_2$ at each boundary, leading to a moment about $\mathbf{D}_3$ which opposes the internal twist of the individual rods in the effective sum $\mathbf{M}$ (30). The contact pressure and forces n_{2i}, given by

$$\mathsf{F}_1 = \frac{4\sin^5(\theta)\csc(4\theta)}{R^3}, \quad \mathsf{n}_{22} = -\mathsf{n}_{21} = \frac{\sin^3(\theta)\sec(2\theta)}{R^2},$$

diverge at $\theta = \pm\pi/4$, *i.e.*, at lock-up. Mathematically this is a result of the ill-definition of the birod manifold past lock-up, physically it would correspond to trying to tighten this braided birod beyond a possible physical limit. In this limit it is necessary to apply an infinitely large pair of equal and opposite forces at the birod's ends in order to maintain the helical structure (it would likely buckle before this limit is reached). This presents an interesting cautionary note. Whilst the effective force $\mathbf{N}$ and moment $\mathbf{M}$ remain finite (zero) in this limit, their constituent components do not. We must always be aware of the fact that though the net force may be zero or small there may still be large forces applied at the boundary by whatever device is used to hold it together. Having given this cautionary note we should also observe that the required pre-twist also diverges in this limit, so it would not have been physically possible to create this divergent state. For the majority of the domain $\theta \in (-\pi/4, \pi/4)$ this model is reasonable.

4.5 The Zeroth Order System:- a Summary

For the purpose of labelling in the perturbation expansion we consider in the next section we shall label all these zeroth order solutions with a superscript (0). The zeroth order variables are

$$\begin{aligned}
&\mathsf{n}_{11}^{(0)} = \mathsf{n}_{12}^{(0)} = 0, \\
&\mathsf{n}_{22}^{(0)} = -\mathsf{n}_{21}^{(0)} = \frac{\sin^3(\theta)\sec(2\theta)}{R^2}, \\
&\mathsf{F}_1^{(0)} = \frac{4\sin^5(\theta)\csc(4\theta)}{R^3}, \\
&\mathsf{n}_{31}^{(0)} = \mathsf{n}_{32}^{(0)} = 0, \\
&\frac{\partial\phi^{(0)}}{\partial s} = \omega = -\frac{\sin(\theta)(\gamma+\sec(2\theta)-1)}{\gamma R}, \\
&\mathsf{U}_1^{(0)} = \mathsf{U}_2^{(0)} = \mathsf{U}_{1r}^{(0)} = \mathsf{U}_{2r}^{(0)} = 0, \\
&\mathsf{U}_3^{(0)} = \frac{\tan(\theta)}{R}, \\
&\mathsf{U}_{3r}^{(0)} = 0, \\
&\lambda_i^{(0)} = \sec(\theta).
\end{aligned} \tag{61}$$

The zeroth order variables for the effective rod frame $\mathsf{U}_{ir}^{(0)}$ are obtained by substitution of the $\mathsf{U}_i^{(0)}$ into (43) - (45). Note that θ has no expansion and hence no labelling, it is the zeroth order form of the angles α_i which we do expand.

5 The Linearised System

In order to consider the changing geometry of the birod's contact line we consider a perturbation of the contact frame. Goriely and Tabor [17] showed the linear correction to the frame can be written in the original basis $\left\{\mathbf{D}_j^{(0)}\right\}$, using a perturbation function $\mathbf{a} = \mathsf{a}_1(s)\mathbf{D}_1^{(0)} + \mathsf{a}_2(s)\mathbf{D}_2^{(0)} + \mathsf{a}_3(s)\mathbf{D}_3^{(0)}$, and writing

$$\mathbf{D}_i \approx \mathbf{D}_i^{(0)} + \epsilon\mathbf{D}_i^{(1)} = \mathbf{D}_i^{(0)} + \epsilon(\mathbf{a}\times\mathbf{D}_i^{(0)}). \tag{62}$$

Under this perturbation scheme the frame's orthonormality is preserved to $\mathcal{O}(\epsilon)$. To be clear the correction to arclength is second order so all the functions in what follows will be parametrised by the arclength of the original birod. The curvatures can be calculated using the following relations

$$\mathsf{U}_1 = \mathbf{D}_3\cdot\mathbf{D}_2', \quad \mathsf{U}_2 = -\mathbf{D}_3\cdot\mathbf{D}_1', \quad \mathsf{U}_3 = \mathbf{D}_2\cdot\mathbf{D}_1', \tag{63}$$

which can be obtained from (11). By expanding the vectors, applying (61), and collecting terms up to first order we obtain

$$\begin{aligned}
\mathsf{U}_1 &\approx \epsilon(\mathsf{a}_1' - \frac{\tan\theta}{R}\mathsf{a}_2), \\
\mathsf{U}_2 &\approx \epsilon(\mathsf{a}_2' + \frac{\tan\theta}{R}\mathsf{a}_1), \\
\mathsf{U}_3 &\approx \frac{\tan(\theta)}{R} + \epsilon\,\mathsf{a}_3'.
\end{aligned} \tag{64}$$

The force vectors are expanded as

$$\mathbf{n}_i \approx \sum_{j=1}^{3}(\mathsf{n}_{ji}^{(0)} + \epsilon\mathsf{n}_{ji}^{(1)})(\mathbf{D}_{ji}^{(0)} + \epsilon(\mathbf{a}\times\mathbf{D}_{ji}^{(0)})), \tag{65}$$

$$\mathbf{F} \approx (\mathsf{F}_1^{(0)} + \epsilon\mathsf{F}_1^{(1)})(\mathbf{D}_1^{(0)} + \epsilon(\mathbf{a}\times\mathbf{D}_1^{(0)})), \tag{66}$$

and the moment vector using

$$\mathbf{m}_i \approx (\mathsf{u}_{1i}^{(0)} + \epsilon \mathsf{u}_{1i}^{(1)})(\mathbf{d}_{1i}^{(0)} + \epsilon \mathbf{d}_{1i}^{(1)}) + (\mathsf{u}_{2i}^{(0)} + \epsilon \mathsf{u}_{2i}^{(1)})(\mathbf{d}_{2i}^{(0)} + \epsilon \mathbf{d}_{2i}^{(1)}) + \gamma(\mathsf{u}_{3i}^{(0)} + \epsilon \mathsf{u}_{3i}^{(1)})(\mathbf{d}_{3i}^{(0)} + \epsilon \mathbf{d}_{3i}^{(1)}). \tag{67}$$

with the expansions for the basis $\mathbf{d}_{ji}$ calculated using (19), (14), (16), the equations for the curvature and torsion (6), the equations for the Frenet vectors (4), (18), and

$$\phi_i \approx \omega s - c + \epsilon \phi_i^{(1)}. \tag{68}$$

The length constraints (17) are expanded using the Leibniz rule, as the limits will change with the change in shape of the birod, to first order we have

$$\begin{aligned} 0 &= \frac{L^{(1)}}{2}\left[\lambda_i^{(0)}(L^{(0)}/2) + \lambda_i^{(0)}(-L^{(0)}/2)\right] + \int_{-L^{(0)}/2}^{L^{(0)}/2} \lambda_i^{(1)}(q)\ \mathrm{d}q, \\ &= L^{(1)}\sec(\theta) + \int_{-L^{(0)}/2}^{L^{(0)}/2} \lambda_i^{(1)}(q)\ \mathrm{d}q. \end{aligned} \tag{69}$$

here q is a dummy parameter representing the arclength of the zeroth order solution and we have used the fact that the L_i are fixed under all deformations due to the individual rod's inextensibility. The integrand is calculated by expanding (16) to first order.

A similar correction must be used for the angles α_i and β_i. By specifying say β_1^+ and β_i^- we make an implicit statement about the correction in length of the contact line through the following relations

$$\alpha_i(L/2) - \alpha_i(-L/2) = \int_{-L/2}^{L/2} \frac{\partial \alpha_i}{\partial q}\ \mathrm{d}q, \quad \beta_i(L/2) - \beta_i(-L/2) = \int_{-L/2}^{-L/2} \frac{\partial \beta_i}{\partial q}\ \mathrm{d}q.$$

Expanding we have

$$\begin{aligned} \alpha_i^{\pm} &= L^{(1)}\left[\frac{\partial \alpha_i^{(0)}}{\partial s}(L^{(0)}/2) + \frac{\partial \alpha_i^{(0)}}{\partial s}(-L^{(0)}/2)\right] + \int_{-L^{(0)}/2}^{L^{(0)}/2} \frac{\partial \alpha_i^{(1)}}{\partial q}\ \mathrm{d}q, \\ &= \frac{L^{(1)}\sin(\theta)(\gamma + \sec(2\theta) - 1)}{\gamma R} + \int_{-L^{(0)}/2}^{L^{(0)}/2} \frac{\partial \alpha_i^{(1)}}{\partial q}\ \mathrm{d}q. \end{aligned} \tag{70}$$

where we have used (61) and we use the notation $\alpha_i^{\pm}$ to denote the total change, incorporating the changing length of the contact line. The corrections to α_i are obtained by expanding (31). For β we have

$$\begin{aligned} \beta_i^{\pm} &= L^{(1)}\left[\frac{\partial b v^{(0)}}{\partial s}(L^{(0)}/2) + \frac{\partial \beta^{(0)}}{\partial s}(-L^{(0)}/2)\right] + \int_{-L^{(0)}/2}^{L^{(0)}/2} \frac{\partial \beta_i^{(1)}}{\partial q}\ \mathrm{d}q, \\ &= \int_{-L^{(0)}/2}^{L^{(0)}/2} \frac{\partial \beta_i^{(1)}}{\partial q}\ \mathrm{d}q. \end{aligned} \tag{71}$$

where we have used (60) and the fact that θ is constant with respect to s, the correction to the angle β is obtained by expanding (32).

In order to automatically include (24) we re-express the balance equations (22) and (23) in sum/difference from *i.e.*,

$$\mathbf{n}_1 - \mathbf{n}_2 + 2\mathbf{F}_1 = 0 \tag{72}$$

$$\mathbf{n}_1 + \mathbf{n}_2 = 0 \tag{73}$$

$$\mathbf{m}_1 - \mathbf{m}_2 + \frac{\mathrm{d}\mathbf{r}_2}{\mathrm{d}s} \times \mathbf{n}_1 - \frac{\mathrm{d}\mathbf{r}_2}{\mathrm{d}s} \times \mathbf{n}_2 = 0 \tag{74}$$

$$\mathbf{m}_1 + \mathbf{m}_2 + \frac{\mathrm{d}\mathbf{r}_2}{\mathrm{d}s} \times \mathbf{n}_1 + \frac{\mathrm{d}\mathbf{r}_2}{\mathrm{d}s} \times \mathbf{n}_2 = 0. \tag{75}$$

The tedious work of inserting the expansions (65), (66) and (67) into (72)-(75), expanding and collecting the $\mathcal{O}(\epsilon)$ terms was performed using symbolic manipulation the resulting equations are given in equations (C.1)-(C.12) of the Appendix. Also in Appendix (C) we detail the procedure by which the ensuing equations are solved. Here we

discuss two linear differential equations which are encountered in solving the system, as their solutions represent two key modes of behaviour inherent to the linearised system. The first is for a_3 and is a fourth order O.D.E

$$\mathsf{a}_3'''' - \frac{(2\cos(2\theta)+\cos(4\theta)+3)\tan^2(\theta)\sec(2\theta)}{R^2}\mathsf{a}_3'' = 0 \tag{76}$$

The coefficient of a_3'' is positive-definite on the domain $\theta \in (-\pi/4, \pi/4)$ so this equation has hyperbolic solutions which are

$$\mathsf{a}_3(s) = C_6 + C_7 s + \frac{R^2\cos(2\theta)\cot^2(\theta)\left(C_8\,\mathrm{e}^{\Theta_1 s} + C_9\,\mathrm{e}^{-\Theta_1 s}\right)}{2\cos(2\theta)+\cos(4\theta)+3}, \tag{77}$$
$$\Theta_1 = \frac{\sec(\theta)\sqrt{-\cos(4\theta)+2\sec(2\theta)-1}}{\sqrt{2}R}.$$

With C_6-C_9 constants of integration. This function is associated with the correction to the twisting through the third of (64). The constant C_7 represents constant change in the twisting of the contact frame, *i.e.*, a constant increase/decrease in helical pitch of the structure. The hyperbolic parts, as we shall see, correspond to dramatic changes in the twisting correction near the boundary. An example of such behaviour is shown in Figure 9(b).

The second equation concerns a_2 and is the following inhomogeneous fourth order O.D.E.

$$\mathsf{a}_2'''' + \frac{2\tan^2(\theta)}{R^2}\mathsf{a}_2'' + \frac{\tan^4(\theta)}{R^4}\mathsf{a}_2 = \Theta_2\left(C_3\sin\left(\frac{s\tan(\theta)}{R}\right) - C_2\cos\left(\frac{s\tan(\theta)}{R}\right)\right), \tag{78}$$
$$\Theta_2 = \frac{(\cos(2\theta)+\cos(4\theta)+2)\tan^2(\theta)\sec(\theta)\sec^2(2\theta)}{2R^2}.$$

In this case the coefficients on the left hand side are positive definite and the general solution has the following form

$$\mathsf{a}_2(s) = (\mathsf{a}_2^{i} + \mathsf{a}_2^{ii}s + \mathsf{a}_2^{iii}s^2)\cos\left(\frac{s\tan(\theta)}{R}\right) + (\mathsf{a}_2^{iv} + \mathsf{a}_2^{v}s + \mathsf{a}_2^{vi}s^2)\sin\left(\frac{s\tan(\theta)}{R}\right), \tag{79}$$
$$\mathsf{a}_2^{i} = -\frac{1}{64}\csc^2(\theta)\sec^2(2\theta)\left(3C_2R^2(5\cos(\theta)+2\cos(3\theta)+\cos(5\theta)) - 16C_{10}(\sin(\theta)-\sin(3\theta))^2\right)$$
$$\mathsf{a}_2^{ii} = C_{11} - \frac{1}{8}C_3R(\cos(2\theta)+\cos(4\theta)+2)\csc(\theta)\sec^2(2\theta), \quad \mathsf{a}_2^{iii} = \frac{1}{8}C_2\left(\sec(\theta)+\cos(\theta)\sec^2(2\theta)\right),$$
$$\mathsf{a}_2^{iv} = \frac{1}{64}\csc^2(\theta)\sec^2(2\theta)\left(16C_{12}(\sin(\theta)-\sin(3\theta))^2 + 3C_3R^2(5\cos(\theta)+2\cos(3\theta)+\cos(5\theta))\right)$$
$$\mathsf{a}_2^{v} = C_{13} - \frac{1}{8}C_2R(\cos(2\theta)+\cos(4\theta)+2)\csc(\theta)\sec^2(2\theta) \quad \mathsf{a}_2^{vi} = -\frac{1}{8}C_3\left(\sec(\theta)+\cos(\theta)\sec^2(2\theta)\right).$$

The function a_1 is composed of the terms which make up a_2. The rate of oscillation of the trigonometric terms is determined by the twist of the original structure. Similar trigonometric terms arise in the linearisation of the single helical rod (see [10]). In that case however there are no linear or quadratic parts to the first order correction of the curvatures of the centreline, thus we see there is a difference in the behaviour of a combined pair of contacting rods, by comparison to two helical rods treated as separate systems. Under the action of moments about $\mathbf{D}_1$ and $\mathbf{D}_2$ the effective rod forms shapes which have a nearly circular bending of the contact line (depicted in Figure 8). By comparison moment induced bending of a single helix yields properly circular bending of the helices centreline (by this we mean the rod centrelines wind with uniform rate on a section of a torus surrounding this centreline).

All other corrections can be written in terms of a_1, a_2 and a_3 with some additional linear terms which result from the various integrations performed during the process of solving the system. We detail the full solutions in the Appendix (equations (D.1)-(D.13)), though their complexity suggests that they only have use for the study of particular interesting limits which can be obtained from them, rather than for their use as a model. In general the accurate treatment of this type of birod system would perhaps best be approached numerically.

6 Effective Rod Constants

The zeroth order terms of both $\mathbf{N}$, $\mathbf{M}$ and the curvatures U_{ir} are zero (see Section 4.5) so we drop the subscript notation of the previous section for what remains. We write $L = L^{(0)}$, the contact line length correction $L^{(1)}$

is denoted L_c, and we remind the reader that the vectors $\{\mathbf{D}_j\}$ and $\{\mathbf{D}_{jr}\}$ are the contact basis of the zeroth order helical configuration (given by (50)-(51)). We denote the extension per unit original length of the contact line as $\mathsf{e} = L_c/L$. The only kinematic changes to the contact line are the curvatures U_{jr} and the extension e and expanding to linear order we have

$$\mathsf{M}_{kr}(\mathsf{U}_{jr}, \mathsf{e}) \approx 0 + \left(\frac{\partial \mathsf{M}_{kr}}{\partial \mathsf{U}_{jr}} \mathsf{U}_{jr} + \frac{\partial \mathsf{M}_{kr}}{\partial \mathsf{e}} \mathsf{e} \right) \epsilon,$$
$$\mathsf{N}_{kr}(\mathsf{U}_{jr}, \mathsf{e}) \approx 0 + \left(\frac{\partial \mathsf{N}_{kr}}{\partial \mathsf{U}_{jc}} \mathsf{U}_{jr} + \frac{\partial \mathsf{N}_{kr}}{\partial \mathsf{e}} \mathsf{e} \right) \epsilon,$$

with the derivatives evaluated at $\mathsf{U}_{jr} = 0, \mathsf{e} = 0, i = 1, 2, 3..$ It is the values of the partial derivatives we wish to obtain, they form a matrix which represents the linear constitutive law of the system. In what follows it will actually be more convenient to obtain the partial derivatives

$$\frac{\partial \mathsf{U}_{jr}}{\partial \mathsf{M}_{kr}}, \quad \frac{\partial \mathsf{U}_{jr}}{\partial \mathsf{N}_{kr}}, \quad \frac{\partial \mathsf{e}}{\partial \mathsf{M}_{kr}}, \quad \frac{\partial \mathsf{e}}{\partial \mathsf{N}_{kr}}.$$

evaluated as the moments and forces vanish.

6.0.1 Orders of L and R

As we are using Kirchhoff model for the individual rods and we allow for significant curvature of the two rods we require that $L/R >> 1$ and $R << 1$ (see Section 3). In what follows it will be convenient to assume that $L \sim \mathcal{O}(1/R)$, $R << 1$. With this the product LR is of order 1. We shall also be assuming the upper bounds used for the sufficiently pinned conditions (40) are of the same order as R, *i.e.*, $\alpha_{im}, \beta_{im} \sim \mathcal{O}(R)$.

6.0.2 Applying the Boundary Conditions

Given we do not enforce specific boundary conditions we instead write our solutions in terms of the corrections $\alpha_1^{(1)}$, $\alpha_2^{(1)}$, $\beta_1^{(1)}$ and $\beta_2^{(1)}$, which would be determined by a specific choice of boundary conditions and constraints. For (40) they must all be less than α_{im}, β_{im}.

If we specify values for these functions at one boundary, say the upper boundary, we can use (70) and (71) in conjunction with specifying the total differences between ends of the birod $\alpha_i^{\pm}$ and $\beta_i^{\pm}$ to obtain values of these quantities on the lower boundary with

$$\alpha_i^{\pm} = \alpha_i(L/2) - \alpha_i(-L/2) + L_c \frac{\sin(\theta)(\gamma + \sec(2\theta) - 1)}{\gamma R},$$
$$\beta_i^{\pm} = \beta_i(L/2) - \beta_i(-L/2).$$

The constraints (40) also ensure the quantities $\alpha_i^{\pm}$ and $\beta_i^{\pm}$ of the same order as R. This is immediately obvious for β_i. In the case of α, the difference $\Delta\alpha_i(B^+) - \Delta\alpha_i(B_i)$ is the net change the total rotation of the pair $(\mathbf{d}_{1i}, \mathbf{d}_{2i})$ with respect to $\mathbf{D}_1$, and it is of order R if the changes $\Delta\alpha_i(B^{\pm})$ are order R, hence the quantities $\alpha_i^{\pm}$ are also required to be of order R.

6.1 Forces

It is shown in Appendix D.1 that the correction to the components to the force $\mathbf{N}_r$ are constant across the birod's length and hence determined by the applied boundary conditions $(\mathsf{N}_{1r}, \mathsf{N}_{2r}, \mathsf{N}_{3r})$.

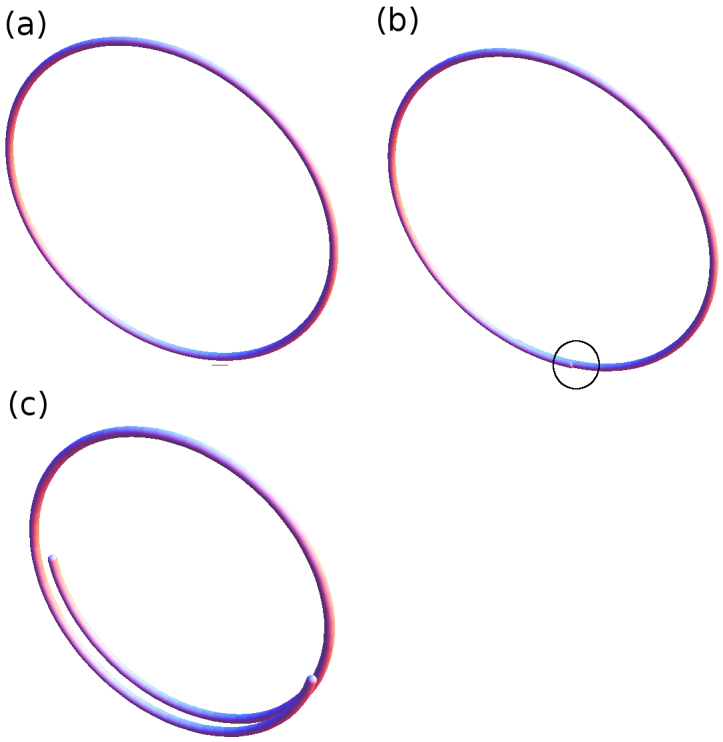

Fig. 8 Depicted are thin tubes representing the contact line of the deformed birod, subject to an applied moment M_{1r}, (linear combinations of M_{1r} and M_{2r} show similar behaviour). The tube widths are the radius $R = 0.1$. Panels (a) and (b) have initial helical angle $\theta = 0.01$ and $\theta = 0.3$ respectively, it is only on the circled section of (b) that we see there is a minor diversion from a circular arc. For the initially much tighter helical structure $\theta = 0.6$ we still see only a small deviation.

6.2 Moments I - the Bending Moment

If $\mathsf{N}_{1r} = \mathsf{N}_{2r} = 0$ the components of the correction to the effective rod moment components M_{1r} and M_{2r} are shown to be constants (Appendix D.2), however, the corrections to the curvatures are not. We first consider the relationship between the curvatures U_{1r} and U_{2r} and the moments M_{1r} and M_{2r}. We have from equation (D.21)

$$\begin{aligned}
\mathsf{U}_{1r}(s) &= A_1 + A_2 \sin\left(\frac{s\tan(\theta)}{R}\right) + A_3 \sin\left(\frac{2s\tan(\theta)}{R}\right) + A_4 \cos\left(\frac{2s\tan(\theta)}{R}\right), \qquad (80)\\
A_1 &= \frac{1}{4}\mathsf{M}_{1r}\left(\sec(\theta) + \cos(\theta)\sec^2(2\theta)\right),\\
A_2 &= \frac{2\mathsf{M}_{2r}R^2\csc(\theta)\sec^2(2\theta)\sin\left(\frac{L\tan(\theta)}{2R}\right)}{2LR},\\
A_3 &= -\frac{1}{4}\mathsf{M}_{2r}(2\sin(\theta) + \sin(3\theta))\tan(\theta)\sec^2(2\theta),\\
A_4 &= -\frac{1}{4}\mathsf{M}_{1r}\sin(\theta)\tan(\theta)\sec(2\theta)(3\sec(2\theta) + 2).
\end{aligned}$$

we see no dependence on M_{3r}, N_{3r} or the kinematic parameters. The same is true of U_{2r}, from equation (D.22) we have

$$\begin{aligned}
\mathsf{U}_{2r}(s) &= A_5 + A_6\cos\left(\frac{s\tan(\theta)}{R}\right) + A_7\sin\left(\frac{2s\tan(\theta)}{R}\right) + A_8\cos\left(\frac{2s\tan(\theta)}{R}\right) \qquad (81)\\
A_5 &= \frac{1}{4}\mathsf{M}_{2r}\left(\sec(\theta)+\cos(\theta)\sec^2(2\theta)\right),\\
A_6 &= -\frac{2\mathsf{M}_{2r}R^2\csc(\theta)\sec^2(2\theta)\sin\left(\frac{L\tan(\theta)}{2R}\right)}{2LR},\\
A_7 &= -\frac{1}{4}\mathsf{M}_{1r}\sin(\theta)\tan(\theta)\sec(2\theta)(3\sec(2\theta)+2),\\
A_8 &= \frac{1}{4}\mathsf{M}_{2r}(2\sin(\theta)+\sin(3\theta))\tan(\theta)\sec^2(2\theta).
\end{aligned}$$

Despite the arclength-varying nature of these expressions we see in Figure 8 that the effective configurations of the deformed contact line do not actually deviate too far from a circular arc if the birod is long and thin. These plots are deliberately exaggerated to make a point (in the sense that this is a linearisation and it applies properly to smaller deformations). In this case we have chosen parameters $L = 30$, $R = 0.1$, and $\theta = 0.01$(a), $0.3(b)$ and 0.6 for(c). These plots were made by varying M_{1r}. Similar behaviour for a linear combination of M_{1r} and M_{2r} is found. It would appear then that there is good reason to take the averaged values of U_{1r} and U_{2r}

$$\bar{\mathsf{U}}_{\alpha r} = \frac{1}{L}\int_{-L/2}^{L/2}\mathsf{U}_{\alpha r}(q)\ \mathrm{d}q, \alpha = 1,2, \qquad (82)$$

as a good measure of the effective constant curvature of the birod under the action of constant moments, at least when the ratio L/R is large. On applying (82) to (80) and (81) we find

$$\begin{aligned}
\bar{\mathsf{U}}_{1r} &= \frac{1}{4}M_1\left(\sec(\theta)+\cos(\theta)\sec^2(2\theta)\right) - \frac{M_1R\sin(\theta)\sec(2\theta)(3\sec(2\theta)+2)\sin\left(\frac{L\tan(\theta)}{R}\right)}{4L},\\
\bar{\mathsf{U}}_{2r} &= \frac{1}{4}M_2\left(\sec(\theta)+\cos(\theta)\sec^2(2\theta)\right)\\
&\quad - \frac{\csc(\theta)\sin\left(\frac{L\tan(\theta)}{2R}\right)\left(2M_2R^2\cot(\theta)\sec^2(2\theta)\sin\left(\frac{L\tan(\theta)}{2R}\right)\right)}{L^2}\\
&\quad + \frac{M_2R(2\sin(\theta)+\sin(3\theta))\sec^2(2\theta)\sin\left(\frac{L\tan(\theta)}{R}\right)}{4L}.
\end{aligned}$$

If we concentrate on $\bar{\mathsf{U}}_{1r}$ briefly we see there are two contributions, the first depends only on the value of M_{1r} and θ, the second also depends on the length and radius of the rod, both algebraically and trigonometrically. The quantity $L\tan(\theta)/R$ is the total helical winding of the birod, its value affects the relative orientation of the vectors $\mathbf{D}_1$ and $\mathbf{D}_{1r}$. Whilst $\mathbf{D}_{1r}(-L/2)$ is parallel to $\mathbf{D}_{1r}(L/2)$ the same is not true of $\mathbf{D}_1$ unless $L\tan(\theta)/R$ is a multiple of 2π. Thus the second quantity depends on the relative orientation of the vectors $\mathbf{D}_1$ at $s = \pm L/2$. If $L\tan(\theta)/R$ is not a multiple of 2π the applied moment M_{1r} at the two ends will have a differing effect on the birod due to the anisotropy of response shown in Figure 3. However, if the birod is thin and $L/R >> 1$ this term will be negligible, in this limit we have

$$\bar{\mathsf{U}}_{1r} \approx \frac{1}{4}\mathsf{M}_{1r}\left(\sec(\theta)+\cos(\theta)\sec^2(2\theta)\right).$$

We note the same trigonometric behaviour appears in the expression for $\bar{\mathsf{U}}_{2r}$, though not in the same form as for $\bar{\mathsf{U}}_{1r}$. This is another manifestation of the anisotropy of response of the birod to applied moments. That said in the limit L/R this effect once again becomes negligible and we have

$$\bar{\mathsf{U}}_{2r} \approx \frac{1}{4}\mathsf{M}_{2r}\left(\sec(\theta)+\cos(\theta)\sec^2(2\theta)\right).$$

With this we see we have the following averaged linear constitutive relationship for the bending moments of the birod

$$\begin{pmatrix}\mathsf{M}_{1r}\\ \mathsf{M}_{2r}\end{pmatrix} = \frac{4}{\sec(\theta)+\cos(\theta)\sec^2(2\theta)}\begin{pmatrix}1&0\\0&1\end{pmatrix}\begin{pmatrix}\mathsf{U}_{1r}\\ \mathsf{U}_{2r}\end{pmatrix}. \qquad (83)$$

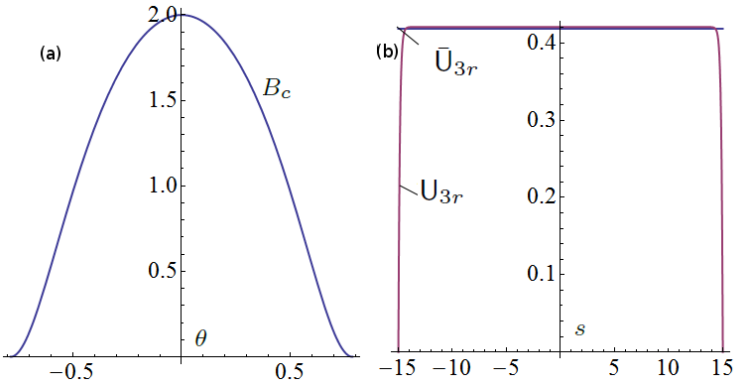

Fig. 9 Panel (a) is a plot of the bending coefficient B_c against θ on the domain $\theta \in [-\pi/4, \pi/4]$. Panel (b) is an example of the function $\mathsf{U}_{3r}(s)$, plotted against s with fully pinned conditions, $L = 30$, $\theta = 0.3$, $R = 0.1$ and $\gamma = 1$ $\mathsf{M}_{3r} = 1$, $\mathsf{N}_{3r} = 1$, we see it is constant for the majority of the domain, with a sharp drop to zero at the boundary. Also plotted is the appropriate averaged value $\hat{\mathsf{U}}_{3r}$ given by (86), we see they overlap for the majority of the domain.

This has the same form as one would expect for an isotropic rod with circular cross-section, *i.e.*, the birods linear bending response is of the same form as its constituent rods. The pre-multiplier is our effective bending coefficient which we label B_c, it is plotted in 9(a) as a function of θ, the initial helical tightness. It does not involve the relative ratio of bending to twisting of the individual rods γ and it is symmetric in θ, hence the same for left-handed and right-handed helical birods. Finally it shows that the birod gets easier to bend as the structure tightens. We should be wary of the limit $\pi/4$ as at this point the divergent $\sec(2\theta)$ would mean (i) we cannot ignore the boundary terms, (ii) the rod would not show the nice almost circular behaviour. But perhaps most importantly the undeformed helical state would have shown divergent behaviour anyway and the linearisation would not have been appropriate.

We should comment on the absence of the ratio γ. In the engineering literature the effective bending coefficients derived depend on γ (see [13]). In these cases however the moment under discussion are the moment applied to the end of the individual rods ($\mathbf{m}_i$) and would thus be more directly influenced by the internal twisting of the rod. This moment would also not take into account the effect of the moment arising from the force difference $\mathbf{n}_1 - \mathbf{n}_2$ of (30). In this note we are interested in the effective moments applied to the rod by some device like the pin device depicted in (Figure 2), and we have found here that, at least to linear order, it is only the tightness of the helical structure through the angle θ which is important. That said we shall see there is a dependency on γ in the torsional response.

6.2.1 Bending with Forces

It is shown in Appendix E that if forces N_{1r} and N_{2r} are applied then the moments M_{1r} and M_{2r} are no longer constant, they have linear behaviour. It is also demonstrated in the presence of forces that the averaged effective moments $\bar{\mathsf{M}}_{\alpha r}$ have the same relationship to the averaged curvatures $\bar{\mathsf{U}}_{\alpha r}$ as demonstrated in the above (under the assumptions detailed in Section 6.0.1). We feel then that the constitutive behaviour (83) is a good effective measure of the bending moment of the system.

6.3 Moments II - the Torsional Response

It is shown in Appendix D.2 that the moment M_{3r} is arclength-constant. The twist of our effective rod U_{3r} (the derivative of (77)) is not constant as a result of the hyperbolic terms. This can lead to extreme changes in pitch of the birod braiding structure near its ends as depicted in Figure 9(b) for a rod of length $L = 30$, and radius $R = 0.1$. We are interested here in the average behaviour of U_{3r} (in the sense of (82)). We see in Figure 9(b) a superposition of the effective average value $\bar{\mathsf{U}}_{3r}$ and the actual twist appear to coincide for the majority of the

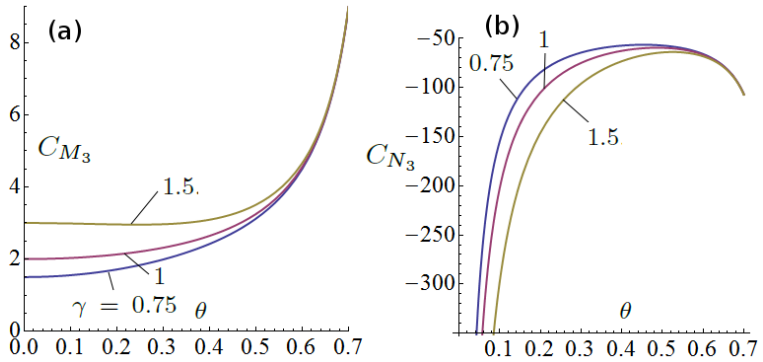

Fig. 10 Plots of the coefficients C_{M_3} and C_{N_3} against the initial helical tightness θ. In (a) we see examples of C_{M_3} with $\gamma = 0.75, 1, 1.5$. For $\gamma = 0.75$ and 1 the coefficient increases with θ with asymptotic behaviour as $\theta \to \pi/4$, for $\gamma = 1.5$ the asymptotic behaviour is still present but the minimum value is for a non-zero θ. In (b) we see the plots of C_{N_3} with θ for $R = 0.1$, there are asymptotes at $\theta = 0$ and $\theta = \pi/4$. We note that the values of C_{N_3} are consistently higher (in magnitude) that those of C_{M_3} except as $\theta \to \pi/4$.

birod's interior. It is is shown in Appendix F that

$$\bar{\mathsf{U}}_{3r} = -\frac{L_c \csc(\theta)\sec(\theta)}{LR}. \tag{84}$$

and

$$L_c = L_c^i \mathsf{M}_{1r} + L_c^{ii}\mathsf{M}_{3r} + L_c^{iii}\mathsf{N}_{1r} + L_c^{iv}\mathsf{N}_{2r} + L_c^{v}\mathsf{N}_{3r} + L_c^{vi}\left(\alpha_1^{\pm} + \alpha_2^{\pm}\right) + L_c^{vii}\beta^{\pm}, \tag{85}$$

$$L_c^i = \frac{8R^2\sin^4(\theta)(2\cos(2\theta)+\cos(4\theta)+3)\sec^{\frac{3}{2}}(2\theta)\sin\left(\frac{L\tan(\theta)}{2R}\right)}{\sqrt{-3\cos(2\theta)-\cos(6\theta)+4}(3(\gamma-1)\cos(2\theta)+(\gamma-1)\cos(6\theta)+4)},$$

$$L_c^{ii} = -\frac{2LR\sin(\theta)\cos(2\theta)}{3(\gamma-1)\cos(2\theta)+(\gamma-1)\cos(6\theta)+4},$$

$$L_c^{iii} = \frac{4R^2\sin^4(\theta)((\cos(4\theta)+3)\sec(2\theta)+2)\left(L\cos\left(\frac{L\tan(\theta)}{2R}\right)-2R\tan(\theta)\sin\left(\frac{L\tan(\theta)}{2R}\right)\right)}{\sqrt{-\cos(2\theta)(3\cos(2\theta)+\cos(6\theta)-4)}(3(\gamma-1)\cos(2\theta)+(\gamma-1)\cos(6\theta)+4)},$$

$$L_c^{iv} = \frac{4LR^2\sin^4(\theta)(2\cos(2\theta)+\cos(4\theta)+3)\sec^{\frac{3}{2}}(2\theta)\sin\left(\frac{L\tan(\theta)}{2R}\right)}{\sqrt{-3\cos(2\theta)-\cos(6\theta)+4}(3(\gamma-1)\cos(2\theta)+(\gamma-1)\cos(6\theta)+4)},$$

$$L_c^{v} = \frac{2LR^2\sin(\theta)\cos(2\theta)\tan(\theta)}{3(\gamma-1)\cos(2\theta)+(\gamma-1)\cos(6\theta)+4},$$

$$L_c^{vi} = -\frac{2\gamma R\sin(\theta)\cos^2(2\theta)}{3(\gamma-1)\cos(2\theta)+(\gamma-1)\cos(6\theta)+4},$$

$$L_c^{vii} = \frac{8R\sin^3(\theta)(2\cos(2\theta)+\cos(4\theta)+3)}{(3(\gamma-1)\cos(2\theta)+(\gamma-1)\cos(6\theta)+4)\sqrt{(-3\cos(2\theta)-\cos(6\theta)+4)\sec(2\theta)}}.$$

Under the assumptions of Section 6.0.1 the leading order term in terms of a series in R is the one involving M_{3r} (L_c^{ii}). This conclusion actually only requires the changes $\alpha_i^{\pm}$ and $\beta^{\pm}$ are of the same order order 1, less stringent than those we have required, we shall see why we chose more conservative constraints shortly.

With this (84) reduces to

$$\bar{\mathsf{U}}_{3r} = \frac{2\cos(2\theta)\sec(\theta)}{3(\gamma-1)\cos(2\theta)+(\gamma-1)\cos(6\theta)+4}\mathsf{M}_{3r}, \tag{86}$$

and the effective torsional stiffness C_{M_3} of the birod would be

$$C_{M_3} = 2\cos(\theta)\left((\gamma-1)\cos^2(2\theta)+\sec(2\theta)\right). \tag{87}$$

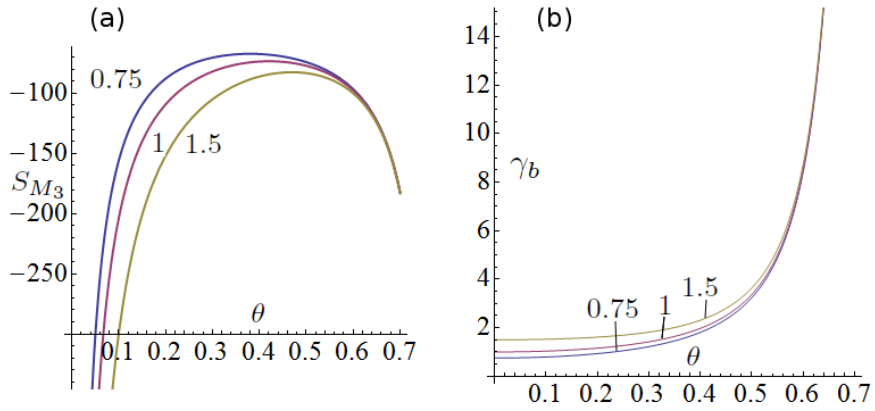

Fig. 11 Panel (a) shows plots of S_{M_3} against θ for $\gamma = 0.75, 1, 1.5$. We see asymptotic behaviour at $\theta \to 0$ and $\theta \to \pi/4$. It is also notable that even at its lowest values the coefficient is of a higher order of magnitude than C_{M_3} as depicted in Figure 10(a). Panel (b) shows plots of the effective twist to bending ratio of the effective rod model of the birod.

For reasons which we shall shortly explain we note the coefficient associated with an axial force N_{3r} would be

$$C_{N_3} = -\frac{2\cos(\theta)\cot(\theta)\left((\gamma-1)\cos^2(2\theta)+\sec(2\theta)\right)}{R}. \tag{88}$$

As shown in Section G of the appendix this is the same behaviour as the linear response of a uniformly helical straight axis birod subjected to a wrench pair $(\mathsf{M}_3, \mathsf{N}_3)$, these coefficients were first derived in [29]. In fact most previous effective rope models haves stiffness matrices which include a coefficient relating U_{3r} to N_3 [13]. If there are no applied forces N_{1r} and N_{2r} and we enforce constraints (40) on the changes in the quantities α_i and β_i then the contributions to L_c associated to the force N_3 (L_c^v) is out on its own as the next order contribution thus yielding the results derived in [29]. Crucially we have found here that this linear constitutive behaviour also holds when the rod is subject to bending moments, *i.e.*, the bending and twisting moments are decoupled.

We have also shown that if we make reasonable assumptions about the boundary constraints used to specify the nature of the pinning device used at the boundaries then the boundary laws have a negligible effect on the large scale mechanical behaviour of the effective rod.

Example plots of the relationship between the coefficients C_{M_3}, C_{N_3} and the value of θ of the initial ply are shown in Figure 10 for the example rod depicted in Figure 8, for which $R = 0.1$. The two most important features of these plots are the asymptotic behaviour of both coefficients as $\theta \to \pi/4$, indicating as expected that it becomes harder to further tighten the birod with the increasing initial tightness (increasing θ value) of the initial helical birod. The second highlights the fact that for small R the coefficient C_{N_3} is much larger than C_{M_3}, providing good reason to ignore the effect of an axial force on the torsional response of the birod.

6.3.1 Contact Line Extension

By dividing (85) by L we obtain an expression for the relative extension e, for which the M_{3r} component will also be the leading order. Once again we also include the N_{3r} term to obtain

$$\mathrm{e} = \frac{2R\sin(\theta)\cos(2\theta)(\mathsf{N}_{3r}R\tan(\theta)-\mathsf{M}_{3r})}{3(\gamma-1)\cos(2\theta)+(\gamma-1)\cos(6\theta)+4} \tag{89}$$

and the effective coefficients S_{M_3}, $S_{\mathsf{N}_{3r}}$ would be

$$\begin{aligned} S_{M_3} &= -\frac{\csc(\theta)(2(\gamma-1)\cos^2(2\theta)+2\sec(2\theta))}{R}, \\ S_{N_3} &= \frac{\cot(\theta)\csc(\theta)\sec(2\theta)(3(\gamma-1)\cos(2\theta)+(\gamma-1)\cos(6\theta)+4)}{2R^2}. \end{aligned} \tag{90}$$

It is shown in the Appendix section G how these same coefficients can be obtained assuming a helical configuration, again this result was previously derived in [29].

The coefficient S_{M_3} is plotted in Figure 11(a) using the same parameters as that of Figure 10, it can be seen that the effective coefficient has a similar asymptotic behaviour to C_{N_3} and has values of an order of magnitude higher than that of C_{M_3} as predicted from (85). This suggests that in the limit $R << 1$ the extension of the contact line is suppressed by comparison to the twisting of the birod.

6.3.2 The Remaining Boundary Conditions

It will have been noted that our expressions do not include the quantities $\alpha_i(L/2)$ and $\beta_i(L/2)$, only the differences $\alpha_i^{\pm}$, $\beta_i^{\pm}$. It is shown in Appendix F that we need further conditions to specify the actual twist correction U_{3r} rather than just its average. In addition there are constants which need to be specified to obtain the complete expressions for the twists $\phi_i^{(1)}$. As this has no effect on the quantities of interest for this particular study we do not pursue this issue any further here.

7 Conclusions

In Sections 2 and 3 we have constructed a birod model for a pair of tubular elastic rods which are in contact. The model focuses on treating the birod composite as a single object by defining its kinematics and dynamics in terms of the changing morphology of the line of mutual contact (section 2.2). The governing mechanical laws of this coupled system are introduced in Section 3. The model is sufficiently general to allow for a varying range of interaction laws at the line of contact, as well as any additional applied body forces/couples. In Section 3.2 we discuss the means by which the interaction laws at the line of contact can be specified, using either constitutive laws or geometric constraints. Finally in Section 3.3 we discuss the application of the boundary conditions through the imposition of geometric constraints and discuss some particularly relevant cases.

In Section 4.2 we discuss the equilibrium state of a birod composed of helically intertwined rods whose contact line is straight. We assume that the interaction at contact is dominated by the normal pressure exerted by the rods on each other. Under these assumptions this is the same model as discussed in [41], though in our case the systems kinematics are expressed in terms of the contact line rather than the individual rods as in [41]. In Section 5 we detail the linearisation procedure used to obtain the linear response of helical birod introduced in Section 4.2. The perturbation scheme is based on the work of Goriely and Tabor [17]. Careful attention is paid to the need to take into account the changing length of the contact line. We discuss the two linear O.D.E's which are encountered in solving the system, the full solution set is to long-winded for the main text and is detailed in Appendix C.

Finally in Section 6.2 we derive the linear response of this helical birod to arbitrary forces and moments. It was shown that if the ratio L/R is large then the effective bending moment of the linearised birod is independent of the boundary conditions used. In Sections 6.3 and 6.3.1 it is shown that if $R << 1$, $L \sim \mathcal{O}(1/R)$ the relative motion of the individual rods at the boundary are restricted so the upper bounds of (40) are of order R, then the effective torsional response coefficients are independent of the particular boundary constraints used. It is also shown that the linear bending and torsional responses of the birod are decoupled. Further it is shown that if R is small then the extension of the birods contact line is suppressed by comparison to the twisting, at least in terms of its linear response, and we propose to treat a birod with the dimensions of a Kirchhoff rod as an effective unstretchable-unshearable rod with the following constitutive law,

$$\begin{pmatrix} \mathsf{M}_{1r} \\ \mathsf{M}_{2r} \\ \mathsf{M}_{3r} \end{pmatrix} = \begin{pmatrix} \frac{4}{\sec(\theta)+\cos(\theta)\sec^2(2\theta)} & 0 & 0 \\ 0 & \frac{4}{\sec(\theta)+\cos(\theta)\sec^2(2\theta)} & 0 \\ 0 & 0 & 2\cos(\theta)\left((\gamma-1)\cos^2(2\theta)+\sec(2\theta)\right) \end{pmatrix} \begin{pmatrix} \bar{\mathsf{U}}_{1r} \\ \bar{\mathsf{U}}_{2r} \\ \bar{\mathsf{U}}_{3r} \end{pmatrix}. \quad (91)$$

With M_{jr} the components of net moment of the contact line (the effective birod) and U_{1r} the averaged curvatures of the contact line. The ratio γ_b, the dimensionless ratio of twisting stiffness over bending stiffness is given by

$$\gamma_b = \frac{B_c}{C_{M_3}} = \frac{1}{16}(\cos(2\theta)+\cos(4\theta)+2)\sec^3(2\theta)(3(\gamma-1)\cos(2\theta)+(\gamma-1)\cos(6\theta)+4). \quad (92)$$

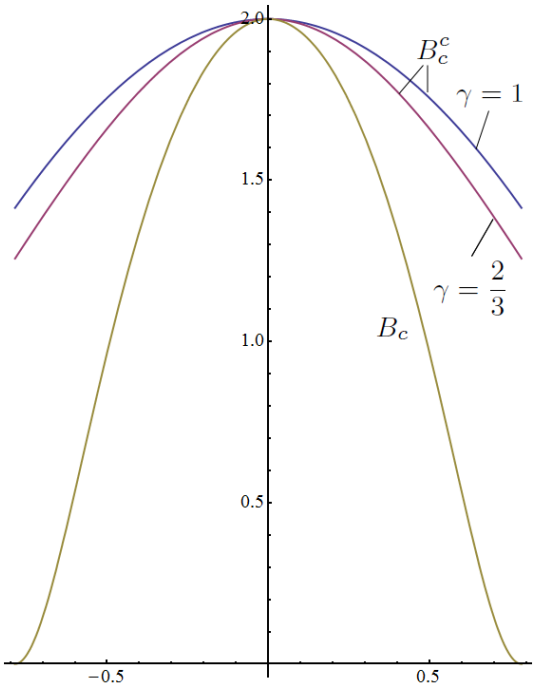

Fig. 12 A comparison of the bending coefficient B_c given by (83) and the Costello [11] bending coefficient (94), plotted for $\gamma = 2/3$ and $\gamma = 1$. The coefficients are plotted as functions of the initial helical angle θ.

Plots of γ_b with θ are shown in Figure 11(b) for values of the rod ratio $\gamma = 0.75, 1, 1.5$[1]. The behaviour is qualitatively similar to the twisting coefficient with the ratio diverging as $\theta \to \pi/4$ when the original helical structure approaches lock-up.

If the ratio $L/R >> 1$ but R is not too small, requiring the curvature is not too large and hence θ small, and we do not consider applying forces N_{1r} and N_{2r}, then the changing length of the contact line becomes important and we propose a linear response of the form

$$\begin{pmatrix} \mathsf{M}_{1r} \\ \mathsf{M}_{2r} \\ \mathsf{M}_{3r} \\ \mathsf{N}_{3r} \end{pmatrix} = \begin{pmatrix} \frac{4}{\sec(\theta)+\cos(\theta)\sec^2(2\theta)} & 0 & 0 & 0 \\ 0 & \frac{4}{\sec(\theta)+\cos(\theta)\sec^2(2\theta)} & 0 & 0 \\ 0 & 0 & C_{M_3} & C_{N_3} \\ 0 & 0 & S_{M_3} & S_{N_3} \end{pmatrix} \begin{pmatrix} \bar{\mathsf{U}}_{1cr} \\ \bar{\mathsf{U}}_{2cr} \\ \bar{\mathsf{U}}_{3cr} \\ \mathrm{e} \end{pmatrix}, \tag{93}$$

with the constants C_{M_3}, C_{N_3}, S_{M_3} and S_{N_3} given by (87), (88) and (90). These constants are the same as those derived in [29], though we have shown here they are applicable even if the birod is subject to bending moments. It was also shown that if the boundary restrictions (40) are assumed then (93) is independent on the particular boundary constraints used.

If the ratio L/R is not large then the constitutional behaviour of the birod would be far more complex and depends on the exact number of helical turns of its initial straight axis state.

7.1 Comparison to Previous Approaches

The homogenization approach of Kehrbaum and Maddocks [21] and Healey [19] considered single elastic rods with helical symmetry and high intrinsic twist. For an isotropic circular rod with the effective bending stiffness is found to be twice the bending coefficient of the rods themselves (2 for the scaling used in (26)). This is the same value as our birod model if $\theta = 0$. Healey considers the most general type of quadratic energy model with this symmetry, and the effective bending coefficients depend on the shearing and coupling moduli of the rod.

[1] Though $\gamma = 1.5$ is outside the range allowed for a single Cosserat rod it would be permissible for a birod composed of linearised birods with constitutive behaviour given by (93).

However, in any of these cases the coefficient does **not** depend on the initial rate of helical winding, so there would be no drop off in the bending coefficient as seen in Figure 9(a), nor does the effective twisting coefficient have the asymptotic behaviour shown in Figure 10(a) as the original structure approaches lock-up. This is a consequence of the fact that the continuum approach does not take into account the finite volume effects of treating the system a two solid contacting rods.

Costello [11] derived the following coefficient for the bending of the centre of rotation of a single helical rod,

$$B_c^c = \frac{2\gamma\cos(\theta)}{2\gamma + (1-\gamma)\sin(\theta)^2}. \tag{94}$$

We assume the birod was composed of two such helical rods with this bending coefficient and plot $2B_c^c$ and our derived bending coefficient against θ for $\gamma = 2/3, 1$ in Figure 12. For small θ the two measures agree, this is a result of the fact that the mutual pressure F_1 is small in this limit. The effect of including the pressure leads the bending coefficient of the birod structure to be significant smaller than two non-interacting rods when this pressure is high. Ramsay [32] extended this work to include the possibility of inter-strand pressure though, its value is based on the incorrect assumption that the rod cross-sections in the plane normal to the rope axis are elliptic. The coefficient does decrease as dramatically as our value as $\theta \to \pi/4$. These two models are the only rope models which include bending coefficients [13]. Notably, none of the torsional or extension coefficients mentioned in the models covered [13] have the asymptotic behaviour shown in Figure 10(a) as lock-up approaches, so the effective ratio of twisting to bending stiffness does not have the asymptotic behaviour shown in Figure 11(b).

7.1.1 An Application of Our Constitutive Law to Actin Filaments

A valuable test of our derived coefficients is by comparison to experimental data of a coiled-coil structure. Actin filaments are know to play a vital role in Eukaryotic Cells. They are coiled-coil molecules and recent experimental evidence suggests the helical shape of the constituent coils has a pitch (P) of approximately 72 nm and a radius of approximately 3 nm [50]. The following relationship

$$P = \frac{2\pi R}{\tan(\theta)}, \tag{95}$$

gives a helical angle $\theta \approx 0.256053$ rad. Studies estimate the measured bending rigidity of Actin to be $(7.3 \pm 4) \times 10^{-26}\,\mathrm{Nm}^2$ [15] and its torsional rigidity to be $(8.0 \pm 1.2) \times 10^{26}\mathrm{Nm}^2$ [45]. This gives a range of possible γ_b values $[0.883177, 1.\dot{3}]$. If we assume the constituent rods of the birod model of Actin are incompressible $\gamma = 2/3$, then 92 would predict a range $\theta \in [0.217577, 0.342496]$, which includes the known value.

A The α_i Boundary Condition of [47]

The second possible pair of conditions given in [47] concern the twisting of the individual rods, either the total twist value U_3 or the twist associated with the function ϕ are fixed for all variations, the authors assume $\mathsf{U}_{31} = \mathsf{U}_{32}$ and $\phi_1 = \phi_2$ so there are only really two conditions. They are

$$\Delta\mathsf{U}_3(\mathcal{P}, \mathcal{P}_0, B^{\pm}) = 0, \text{ or. } \Delta\phi(\mathcal{P}, \mathcal{P}_0, B^{\pm}) = 0.$$

We can translate these into a conditions on β as follows. We differentiate (31) using (2) and (11) to obtain

$$\mathbf{D}_1' = (\alpha_1' - \lambda_i\mathsf{U}_{31})(\cos(\alpha_i)\mathbf{d}_{1i} - \sin(\alpha_i)\mathbf{d}_{2i}) + \lambda_i(\cos(\alpha_i)\mathsf{U}_{1i} - \sin(\alpha_i)\mathsf{U}_{2i})\mathbf{d}_{31}.$$

The $\mathbf{D}_1$ component of the R.H.S must be zero. It can be shown that when the birod takes on the general helical form (13) that this condition can be satisfied if

$$\alpha_i' = -(\lambda_i\tau + \phi'), \text{or, } \alpha_i = -\phi.$$

giving the required conditions.

B Solving the Zeroth Order Equilibrium Equations

Substituting (50-52) and (49) into the moment vector (26) we have

$$\begin{aligned}\mathbf{m}_i = (-1)^{i+1}\frac{\sin(\theta)\cos(\theta)\left((\gamma-1)\sin(\theta) + \gamma R\phi_i'(s)\right)}{R}\mathbf{D}_2 \\ + \frac{\sin(\theta)((\gamma-1)\cos(2\theta) + \gamma + 1) + 2\gamma R\cos^2(\theta)\phi_i'}{2R}\mathbf{D}_3.\end{aligned} \tag{B.1}$$

Substituting (28), the moment vector (B.1) and (15) into (23), with $\mathsf{U}_1 = \mathsf{U}_2 = 0$ and $\nu_0 = \tan(\theta)/R$, we obtain the following equations for rod 1

$$-(\gamma-1)\sin^3(\theta) + R\left(R\mathsf{n}_{21} - R\tan(\theta)\mathsf{n}_{31} + \gamma\sin^2(\theta)\phi_1'\right) = 0, \tag{B.2}$$

$$\mathsf{n}_{11}(s) + \gamma\sin(\theta)\cos(\theta)\phi_1'' = 0, \tag{B.3}$$

$$\gamma\cos^2(\theta)\phi_1'' - \tan(\theta)\mathsf{n}_{11} = 0. \tag{B.4}$$

With the three equations corresponding to the $\mathbf{D}_1$, $\mathbf{D}_2$ and $\mathbf{D}_3$ components of (23) respectively. And for rod 2 we have

$$(1-\gamma)\sin^3(\theta) + R\left(-R(\mathsf{n}_{22} + \tan(\theta)\mathsf{n}_{32}) + \gamma\sin^2(\theta)\phi_2'\right) = 0, \tag{B.5}$$

$$\mathsf{n}_{12}(s) - \gamma\sin(\theta)\cos(\theta)\phi_2'' = 0, \tag{B.6}$$

$$\gamma\cos^2(\theta)\phi_2'' + \tan(\theta)\mathsf{n}_{12} = 0. \tag{B.7}$$

Substituting (28) into the force equations (22), using $\mathbf{F}_1 = -\mathbf{F}_2 = \mathbf{F}$ and using (15) we obtain

$$\begin{aligned} \mathsf{F}_1 - \mathsf{n}_{21}\tfrac{\tan(\theta)}{R} + \mathsf{n}_{11}' = 0, \quad & -\mathsf{F}_1 - \mathsf{n}_{22}\tfrac{\tan(\theta)}{R} + \mathsf{n}_{12}' = 0 \\ \mathsf{n}_{11}\tfrac{\tan(\theta)}{R} + \mathsf{n}_{21}' = 0, \quad & \mathsf{n}_{12}\tfrac{\tan(\theta)}{R} + \mathsf{n}_{22}' = 0 \\ \mathsf{n}_{31}' = 0, \quad & \mathsf{n}_{32}' = 0 \end{aligned} \tag{B.8}$$

With the equations on the left being those of the first rod and those on the right of the second rod. We have used $\mathsf{F}_2 = -\mathsf{F}_1$ from (24). The third line of equations imply n_{31} and n_{32} are constant.

It is known that for rods with the particular linear form of moment vector we use that $\mathsf{u}_{3i}' = 0$ and the twist is linear, *e.g.*, [30]. In this case as the torsion of the rods is constant and this implies that $\phi_1'' = \phi_2'' = 0$, and from (B.3) and (B.6) we have that $\mathsf{n}_{11}(s) = \mathsf{n}_{12}(s) = 0$, which also satisfies (B.4) and (B.7). So we can write

$$\phi_1 = \omega_1 s + c_1, \quad \phi_2' = \omega_2 s + c_2. \tag{B.9}$$

With the constants (c_1, c_2) determined by the relative orientation of the pairs $(\mathbf{d}_{1i}, \mathbf{d}_{2i})$ with respect to the Cartesian basis at $s = 0$. They do not feature in the following analysis. With this constant rate and the fact that $\mathsf{n}_{11} = \mathsf{n}_{12} = 0$, the equations on the second line of (B.8) imply that n_{21} and n_{22} are constant and the first line gives us the following

$$\mathsf{n}_{21}(s) = R\mathsf{F}_1\cot(\theta), \quad \mathsf{n}_{22}(s) = -R\mathsf{F}_1\cot(\theta), \quad \mathsf{n}_{21} = -\mathsf{n}_{22}. \tag{B.10}$$

so F_1 is also constant. Finally from (B.2) and (B.3) we obtain

$$\mathsf{n}_{31} = \frac{R^3\mathsf{F}_1\cot^2(\theta) + \sin(\theta)\cos(\theta)((\gamma-1)\sin(\theta) + \gamma R\omega_1)}{R^2}, \tag{B.11}$$

$$\mathsf{n}_{32} = \frac{R^3\mathsf{F}_1\cot^2(\theta) + \sin(\theta)\cos(\theta)((\gamma-1)\sin(\theta) + \gamma R\omega_2)}{R^2}. \tag{B.12}$$

Using $n_{1i} = 0$ and substituting (B.10), (B.11) and (B.12) into 29 and 30 we obtain respectively (53) and (C.1). Substituting (B.9) into (B.1) we obtain expressions for $\mathbf{m}_1$ and $\mathbf{m}_2$. Substituting these expressions and (54) into (30) we obtain (55).

C Solving the first-order system

In what follows all unknown functions will be the order ϵ corrections of the expansion detailed in Section 5 of the main document, as such we shall drop the superscript notation i.e. $\mathsf{n}_i^{(1)}$ will simply be denoted n_i. Expressed in full the majority of the functions are quite substantial in terms of the length on the page. However, much of this complexity arises from terms which have no dependence on s, only the characteristic values of the undeformed state of the birod θ, γ and R. For clarity we do not detail these expressions in this document, except where necessary. This choice is made to clearly highlight the functional s-dependence of each function and map out the various steps by which the system can be solved. The full forms are available to the interested readers who are invited to contact the author to obtain them.

We have chosen to label these constant terms in the same form as the function itself with a roman numeral superscript. For example the function n_{31} is shown to be

$$\mathsf{n}_{31}(s) = \mathsf{n}_{31}^{i} + \left(\mathsf{n}_{31}^{ii} + \mathsf{n}_{31}^{iii}s\right)\cos\left(\frac{s\tan(\theta)}{R}\right) + \left(\mathsf{n}_{31}^{iv} + \mathsf{n}_{31}^{v}s\right)\sin\left(\frac{s\tan(\theta)}{R}\right),$$

with the terms $\mathsf{n}_{31}^{l},\ l = i, \ldots v$ having no $s-$ dependence whose exact for is omitted form this document.

Applying (11), (64), (65) and (66) to (72) and collecting the order ϵ terms we obtain the following three equations,

$$R\left(R\left(2\mathsf{F}_1 + \mathsf{n}_{11}' - \mathsf{n}_{12}'\right) + \tan(\theta)(\mathsf{n}_{22} - \mathsf{n}_{21})\right) - 2\sin^3(\theta)\sec(2\theta)\mathsf{a}_3' = 0, \tag{C.1}$$

$$\tan(\theta)(\mathsf{n}_{11} - \mathsf{n}_{12}) + R\left(\mathsf{n}_{21}' - \mathsf{n}_{22}'\right) = 0, \tag{C.2}$$

$$R^3\left(\mathsf{n}_{31}'(s) - \mathsf{n}_{32}'\right) + 2\sin^3(\theta)\sec(2\theta)\left(R\mathsf{a}_1'(s) - \tan(\theta)\mathsf{a}_2\right). \tag{C.3}$$

Applying (11), (64), (65) and (66) to (73) and collecting the order ϵ terms we obtain the following three equations,

$$R\left(\mathsf{n}_{11}'(s)+\mathsf{n}_{12}'(s)\right)-\tan(\theta)(\mathsf{n}_{21}+\mathsf{n}_{22})=0, \tag{C.4}$$

$$\tan(\theta)(\mathsf{n}_{11}+\mathsf{n}_{12})+R\left(\mathsf{n}_{21}'+\mathsf{n}_{22}'\right)=0, \tag{C.5}$$

$$\mathsf{n}_{31}'+\mathsf{n}_{32}'=0. \tag{C.6}$$

Applying the moment difference equations (11), (64), (65) and (67) to (74) and collecting the order ϵ terms we obtain the following three equations.

$$\mathsf{n}_{21}+\mathsf{n}_{22}+\tan(\theta)(\mathsf{n}_{31}+\mathsf{n}_{32})+\mathsf{m}_{d1}^{i}\mathsf{a}_3^{(3)}+\mathsf{m}_{d1}^{ii}\mathsf{a}_3'-\frac{\gamma\sin^2(\theta)}{R}(\phi_1'+\phi_2')=0, \tag{C.7}$$

$$\mathsf{n}_{11}-\mathsf{n}_{12}+\mathsf{m}_{d2}^{i}\mathsf{a}_3^{(4)}+\mathsf{m}_{d2}^{ii}\mathsf{a}_3''+\gamma\sin(\theta)\cos(\theta)(\phi_1''+\phi_2'')=0 \tag{C.8}$$

$$-\tan(\theta)(\mathsf{n}_{11}+\mathsf{n}_{12})+\mathsf{m}_{d3}^{i}\mathsf{a}_2^{(4)}+\mathsf{m}_{d3}^{ii}\mathsf{a}_2+\mathsf{m}_{d3}^{iii}\mathsf{a}_1^{(3)}+\mathsf{m}_{d3}^{iv}\mathsf{a}_1'+\mathsf{m}_{d3}^{v}\mathsf{a}_2''+\gamma\cos^2(\theta)(\phi_1''-\phi_2'')=0. \tag{C.9}$$

The terms m_{di}^{l} (difference) are the arclength constant terms which we omit for brevity. Finally applying the moment sum equations (11), (64), (65) and (67) to (75) and collecting the order ϵ terms we obtain the following three equations.

$$-\mathsf{n}_{21}-\mathsf{n}_{22}+\tan(\theta)(\mathsf{n}_{31}-\mathsf{n}_{32})+\mathsf{m}_{s1}^{i}\mathsf{a}_1+\mathsf{m}_{s1}^{ii}\mathsf{a}_2^{(3)}+\mathsf{m}_{s1}^{iii}\mathsf{a}_2'-\frac{\gamma\sin^2(\theta)}{R}(\phi_1'-\phi_2)+\mathsf{m}_{s1}^{iv}\mathsf{a}_1''=0, \tag{C.10}$$

$$\mathsf{n}_{11}+\mathsf{n}_{12}+\mathsf{m}_{s2}^{i}\mathsf{a}_2+\mathsf{m}_{s2}^{ii}\mathsf{a}_1^{(3)}+\mathsf{m}_{s2}^{iii}\mathsf{a}_1'+\mathsf{m}_{s2}^{iv}\mathsf{a}_2''+\gamma\sin(\theta)\cos(\theta)(\phi_1''-\phi_2'')+\mathsf{m}_{s2}^{v}\mathsf{a}_2^{(4)}=0, \tag{C.11}$$

$$\tan(\theta)(\mathsf{n}_{12}-\mathsf{n}_{11})+\mathsf{m}_{s3}^{i}\mathsf{a}_3''+\mathsf{m}_{s3}^{ii}\mathsf{a}_3^{(4)}+\gamma\cos^2(\theta)(\phi_1''+\phi_2'')=0. \tag{C.12}$$

The terms m_{di}^{l} (sum) are the arclength constant terms which we omit for brevity. To begin solving, from (C.6) we have

$$\mathsf{n}_{31}=C_1-\mathsf{n}_{32}.$$

with C_1 an arbitrary constant of integration, in what follows all constants of integration will be labelled C_i. It can also be shown that (C.4) and (C.5) are satisfied generally if

$$\mathsf{n}_{22}(s)=C_2\sin\left(\frac{\tan(\theta)}{R}s\right)+C_3\cos\left(\frac{\tan(\theta)}{R}s\right)-\mathsf{n}_{21}(s),$$
$$\mathsf{n}_{11}(s)=C_3\sin\left(\frac{\tan(\theta)}{R}s\right)-C_2\cos\left(\frac{\tan(\theta)}{R}s\right)-\mathsf{n}_{12}(s).$$

Our next step is to obtain an equation for a_3. We use (C.10) to eliminate n_{32}. We then use (C.7) to eliminate n_{21} and (C.8) to eliminate n_{12}. Having followed these steps (C.2) is reduced to an equation which can be integrated twice to eliminate ϕ_2. Finally, substituting this expression for ϕ_2 into (C.12) and using the full forms of the various constant expressions introduced, we obtain the following fourth order O.D.E

$$\mathsf{a}_3''''-\frac{(2\cos(2\theta)+\cos(4\theta)+3)\tan^2(\theta)\sec(2\theta)}{R^2}\mathsf{a}_3''=0$$

The coefficient of a_3'' is positive-definite on the domain $\theta\in(-\pi/4,\pi/4)$ so this equation has hyperbolic solutions which are

$$\mathsf{a}_3(s)=C_6+C_7s+\frac{R^2\cos(2\theta)\cot^2(\theta)}{2\cos(2\theta)+\cos(4\theta)+3}\left(C_8\,\mathrm{e}^{\Theta_1 s}+C_9\,\mathrm{e}^{-\Theta_1 s}\right), \tag{C.13}$$

$$\Theta_1=\frac{\sec(\theta)\sqrt{-\cos(4\theta)+2\sec(2\theta)-1}}{\sqrt{2}R}.$$

At this point we take stock, we have eliminated all the force terms, ϕ_2 and a_3, using equations (C.2), (C.4), (C.5), (C.6), (C.7), (C.8), (C.10), and (C.12). The remaining functions are

$$\mathsf{a}_1,\quad \mathsf{a}_2,\quad \phi_1,\text{ and }\mathsf{F}_1.$$

and the remaining equations (C.1), (C.3), (C.9) and (C.11).

The linear combination of equations $\sin(\theta)$(C.9) - $\cos(\theta)$(C.11), (C.3)$R-$(C.11), and $\cos(\theta)$(C.8) + $\sin(\theta)$(C.11) yield respectively the equations

$$\sec(\theta)\left(C_2\cos\left(\frac{s\tan(\theta)}{R}\right)-C_3\sin\left(\frac{s\tan(\theta)}{R}\right)\right)+\frac{(\sec(2\theta)-1)\mathsf{a}_2}{R^2}-\frac{(\cos(2\theta)+\cos(4\theta)+2)\tan(2\theta)\mathsf{a}_1'}{2R}$$
$$+\cos^2(\theta)(-(\cos(4\theta)\sec(2\theta)+1))\mathsf{a}_2''=0 \tag{C.14}$$

$$2C_2\cos\left(\frac{s\tan(\theta)}{R}\right)-2C_3\sin\left(\frac{s\tan(\theta)}{R}\right)+2R^2\cos^3(\theta)\mathsf{a}_2^{(4)}+\frac{2\sin(\theta)\tan(\theta)\mathsf{a}_2}{R^2}-2R\cos^3(\theta)\cot(\theta)\mathsf{a}_1^{(3)}$$
$$-\frac{2\sin(\theta)\cos^2(\theta)\mathsf{a}_1'}{R}+\frac{1}{2}(5\cos(\theta)-\cos(3\theta))\mathsf{a}_2''=0. \tag{C.15}$$

$$-2\gamma R^2\cos^2(\theta)\cot(\theta)\mathsf{a}_2^{(4)}+2\gamma R\cos^2(\theta)\cot^2(\theta)\mathsf{a}_1^{(3)}(s)+\frac{2\sin^2(\theta)\cos^2(\theta)(\gamma-\sec(2\theta)+1)\mathsf{a}_1'}{R}$$
$$-\frac{1}{8}\cot(\theta)\sec(2\theta)((15\gamma-1)\cos(2\theta)+(\gamma+1)\cos(6\theta)-2\cos(4\theta)+2)\mathsf{a}_2''+2\gamma\cos(\theta)\phi_1''=0 \tag{C.16}$$

Using (C.14) we can obtain expressions for a_1' and a_1''' in terms of a_2 and its derivatives. Substituting this into (C.15) we obtain the following inhomogeneous fourth order O.D.E.

$$\mathsf{a}_2'''' + \frac{2\tan^2(\theta)}{R^2}\mathsf{a}_2'' + \frac{\tan^4(\theta)}{R^4}\mathsf{a}_2 = \Theta_2\left(\mathrm{C3}\sin\left(\frac{s\tan(\theta)}{R}\right) - C_2\cos\left(\frac{s\tan(\theta)}{R}\right)\right),$$
$$\Theta_2 = \frac{(\cos(2\theta)+\cos(4\theta)+2)\tan^2(\theta)\sec(\theta)\sec^2(2\theta)}{2R^2}.$$

In this case the coefficients on the left hand side are positive definite and the general solution has the following form

$$\mathsf{a}_2(s) = (\mathsf{a}_2^i + \mathsf{a}_2^{ii}s + \mathsf{a}_2^{iii}s^2)\cos\left(\frac{s\tan(\theta)}{R}\right) + (\mathsf{a}_2^{iv} + \mathsf{a}_2^{v}s + \mathsf{a}_2^{vi}s^2)\sin\left(\frac{s\tan(\theta)}{R}\right). \tag{C.17}$$

We can now use (C.14) to obtain a final expression for a_1, it only appears as a first derivative so all that is required is a single integration (the final expression is shown in (D.13)). Inserting the expressions for a_1 and a_2 into (C.16), we then integrate twice to obtain an expression for ϕ_2 (D.12). Finally we can use (C.1) to obtain our expression for F_1 (D.10).

D The corrected system

As in C the final expressions written out in full are somewhat substantial. Once again we only highlight the functional s-dependence of each function and label the parts of the final expressions which are constant in s using the roman numeral system introduced in section C. The final forms of the solutions to the system (C.1)- (C.12) are

$$\mathsf{n}_{11}(s) = -\frac{1}{2}\left(C_2\cos\left(\frac{s\tan(\theta)}{R}\right) + C_3\sin\left(\frac{s\tan(\theta)}{R}\right)\right) + \sin(\theta)\cos^4(\theta)(\sec(2\theta)+2)\left(C_8\,\mathrm{e}^{\Theta_1 s} + C_9\,\mathrm{e}^{-\Theta_1 s}\right), \tag{D.1}$$

$$\mathsf{n}_{12}(s) = -\frac{1}{2}C_2\cos\left(\frac{s\tan(\theta)}{R}\right) + \frac{1}{2}C_3\sin\left(\frac{s\tan(\theta)}{R}\right) - \sin(\theta)\cos^4(\theta)(\sec(2\theta)+2)\left(C_8\,\mathrm{e}^{\Theta_1 s} + C_9\,\mathrm{e}^{-\Theta_1 s}\right), \tag{D.2}$$

$$\mathsf{n}_{21}(s) = \mathsf{n}_{21}^i + \frac{1}{2}\left(C_2\sin\left(\frac{s\tan(\theta)}{R}\right) + C_3\cos\left(\frac{s\tan(\theta)}{R}\right)\right) - \mathsf{n}_{21}^{ii}\left(C_8\,\mathrm{e}^{\Theta_1 s} - C_9\,\mathrm{e}^{-\Theta_1 s}\right), \tag{D.3}$$

$$\mathsf{n}_{22}(s) = \mathsf{n}_{22}^i + \frac{1}{2}\left(C_2\sin\left(\frac{s\tan(\theta)}{R}\right) + C_3\cos\left(\frac{s\tan(\theta)}{R}\right)\right) + \mathsf{n}_{22}^{ii}\left(C_8\,\mathrm{e}^{\Theta_1 s} - C_9\,\mathrm{e}^{-\Theta_1 s}\right), \tag{D.4}$$

$$\mathsf{n}_{31}(s) = \mathsf{n}_{31}^i + (\mathsf{n}_{31}^{ii} + \mathsf{n}_{31}^{iii}s)\cos\left(\frac{s\tan(\theta)}{R}\right) + (\mathsf{n}_{31}^{iv} + \mathsf{n}_{31}^{v}s)\sin\left(\frac{s\tan(\theta)}{R}\right) \tag{D.5}$$

$$\mathsf{n}_{32}(s) = \mathsf{n}_{32}^i + (\mathsf{n}_{32}^{ii} + \mathsf{n}_{32}^{iii}s)\cos\left(\frac{s\tan(\theta)}{R}\right) + (\mathsf{n}_{32}^{iv} + \mathsf{n}_{32}^{v}s)\sin\left(\frac{s\tan(\theta)}{R}\right), \tag{D.6}$$

$$\mathsf{U}_1(s) = (\mathsf{U}_1^i + \mathsf{U}_1^{ii}s)\cos\left(\frac{s\tan(\theta)}{R}\right) + (\mathsf{U}_1^{iii} + \mathsf{U}_1^{iv}s)\sin\left(\frac{s\tan(\theta)}{R}\right), \tag{D.7}$$

$$\mathsf{U}_2(s) = (\mathsf{U}_2^i + \mathsf{U}_2^{ii}s)\cos\left(\frac{s\tan(\theta)}{R}\right) + (\mathsf{U}_2^{iii} + \mathsf{U}_2^{iv}s)\sin\left(\frac{s\tan(\theta)}{R}\right) + \mathsf{U}_2^{v}, \tag{D.8}$$

$$\mathsf{U}_3(s) = C_7 + \mathsf{U}_3^i\left(C_8\,\mathrm{e}^{\Theta_1 s} + C_9\,\mathrm{e}^{-\Theta_1 s}\right), \tag{D.9}$$

$$\mathsf{F}_1(s) = \mathsf{F}_1^i + \mathsf{F}_1^{ii}\left(C_8\,\mathrm{e}^{\Theta_1 s} - C_9\,\mathrm{e}^{-\Theta_1 s}\right), \tag{D.10}$$

$$\phi_1(s) = (\phi_1^i + \phi_1^{ii}s)\cos\left(\frac{s\tan(\theta)}{R}\right) + (\phi_1^{iii} + \phi_1^{iv}s)\sin\left(\frac{s\tan(\theta)}{R}\right) + \phi_1^v\left(C_8\,\mathrm{e}^{\Theta_1 s} + C_9\,\mathrm{e}^{-\Theta_1 s}\right) + C_{15}s + C_{16}, \tag{D.11}$$

$$\phi_2(s) = (\phi_2^i + \phi_2^{ii}s)\cos\left(\frac{s\tan(\theta)}{R}\right) + (\phi_2^{iii} + \phi_2^{iv}s)\sin\left(\frac{s\tan(\theta)}{R}\right) + \phi_2^v\left(C_8\,\mathrm{e}^{\Theta_1 s} + C_9\,\mathrm{e}^{-\Theta_1 s}\right) + \phi_2^{vi} + \phi_2^{vii}s, \tag{D.12}$$

$$\mathsf{a}_1(s) = (\mathsf{a}_1^i + \mathsf{a}_1^{ii}s)\cos\left(\frac{s\tan(\theta)}{R}\right) + (\mathsf{a}_1^{iii} + \mathsf{a}_1^{iv}s)\sin\left(\frac{s\tan(\theta)}{R}\right) + C_{14}. \tag{D.13}$$

in conjunction with (C.17) and (C.13). In addition by expanding (31) and (32) and comparing the order ϵ terms to the expansion for $\mathbf{D}_1$ and $\mathbf{d}_{3i}$ we obtain the following expressions for the corrections to the angles α_i and β_i

$$\alpha_1 = (\alpha_1^i + \alpha_1^{ii}s)\cos\left(\frac{s\tan(\theta)}{R}\right) + (\alpha_1^i + \alpha_1^{ii}s)\sin\left(\frac{s\tan(\theta)}{R}\right) + \alpha_1^{iii}\left(C_8\,\mathrm{e}^{\Theta_1 s} + C_9\,\mathrm{e}^{-\Theta_1 s}\right) - C_{15}s - C_{16}, \tag{D.14}$$

$$\alpha_2 = (\alpha_2^i + \alpha_2^{ii}s)\cos\left(\frac{s\tan(\theta)}{R}\right) + (\alpha_2^{iii} + \alpha_2^{iv}s)\sin\left(\frac{s\tan(\theta)}{R}\right) + \alpha_2^v\left(C_8\,\mathrm{e}^{\Theta_1 s} + C_9\,\mathrm{e}^{-\Theta_1 s}\right)\alpha_2^{vi}s - \alpha_2^{vii}, \tag{D.15}$$

$$\beta_1 = (\beta_1^i + \beta_1^{ii}s)\cos\left(\frac{s\tan(\theta)}{R}\right) + (\beta_1^{iii} + \beta_1^{iv}s+)\sin\left(\frac{s\tan(\theta)}{R}\right) + \beta_1^v\left(C_8\,\mathrm{e}^{\Theta_1 s} - C_9\,\mathrm{e}^{-\Theta_1 s}\right) + \beta_1^{vi}, \tag{D.16}$$

$$\beta_2 = (\beta_2^i + \beta_2^{ii}s)\cos\left(\frac{s\tan(\theta)}{R}\right) + (\beta_2^{iii} + \beta_2^{iv}s)\sin\left(\frac{s\tan(\theta)}{R}\right) + \beta_2^v\left(C_8\,\mathrm{e}^{\Theta_1 s} - C_9\,\mathrm{e}^{-\Theta_1 s}\right) + \beta_2^{vi}. \tag{D.17}$$

Finally the corrections $\lambda_i^{(1)}$ can be integrated leading to expressions for the quantity

$$s_{ic}(s) = \int_{-L/2}^{L/2} \lambda_i^{(1)}(q)\ \mathrm{d}q. \tag{D.18}$$

with

$$s_{1c}(s) = \left(s_{1c}^{i} + s_{1c}^{ii}s\right)\cos\left(\frac{s\tan(\theta)}{R}\right) + \left(s_{1c}^{iii} + s_{1c}^{iv}s+\right)\sin\left(\frac{s\tan(\theta)}{R}\right) + s_{1c}^{v}\left(C_8\,\mathrm{e}^{\Theta_1 s} + C_9\,\mathrm{e}^{-\Theta_1 s}\right) + s_{1c}^{vi}s + C_{17}, \tag{D.19}$$

$$s_{2c}(s) = \left(s_{2c}^{i} + s_{2c}^{ii}s\right)\cos\left(\frac{s\tan(\theta)}{R}\right) + \left(s_{2c}^{iii} + s_{2c}^{iv}s+\right)\sin\left(\frac{s\tan(\theta)}{R}\right) + s_{2c}^{v}\left(C_8\,\mathrm{e}^{\Theta_1 s} + C_9\,\mathrm{e}^{-\Theta_1 s}\right) + s_{2c}^{vi}s + C_{18}.$$

D.1 Birod forces

Applying (C.13), (D.1)-(D.6), (D.13) and (C.17) to (65) we obtain the corrections to the force vectors $\mathbf{n}_i$. Using (29), (46) and the fact that the zeroth order birod forces N_{jr} are zero, we obtain the following expressions for the effective birod forces $\mathbf{N}_{ir}$

$$\begin{aligned}\mathsf{N}_{1r} &= -C_2,\\ \mathsf{N}_{2r} &= C_3,\\ \mathsf{N}_{3r} &= C_1.\end{aligned} \tag{D.20}$$

D.2 Birod Moments

Applying (C.13), (C.17) and (D.7)-(D.13) to (67) we obtain the corrections to the moment vectors $\mathbf{m}_i$. Using (30), (46), and the fact that the zeroth order birod moments M_{jr} are zero we obtain expressions for the effective birod moments $\mathbf{M}_{ir}$. With a little algebra it we see there is no ensuing trigonometric dependence on s. Finally, using (D.20) and the exact forms of the various constants we have introduced, we arrive at the following expressions

$$\mathsf{M}_{1r}(s) = -\frac{\csc(\theta)(4C_{13}(\sin(2\theta)+\sin(6\theta)) + \mathsf{N}_{1r}R(9\cos(\theta)+6\cos(3\theta)+\cos(5\theta)) - 2\mathsf{N}_{2r}s(3\sin(\theta)+\sin(5\theta)))}{4(\cos(2\theta)+\cos(4\theta)+2)}, \tag{D.21}$$

$$\mathsf{M}_{2r}(s) = -\frac{\csc(\theta)(-4C_{11}(\sin(2\theta)+\sin(6\theta)) + 2\mathsf{N}_{1r}s(3\sin(\theta)+\sin(5\theta)) + \mathsf{N}_{2r}R(9\cos(\theta)+6\cos(3\theta)+\cos(5\theta)))}{4(\cos(2\theta)+\cos(4\theta)+2)}, \tag{D.22}$$

$$\mathsf{M}_{3r} = \mathsf{N}_{3r}R\tan(\theta) + \gamma C_4\cos(2\theta) + C_7(\cos(3\theta)+\cos(\theta)(2\sec(2\theta)+3)). \tag{D.23}$$

We note that M_{3r} is constant and in the absence of forces N_{1r} and N_{2r}, M_{1r} and M_{2r} are also constant.

D.3 Enforcing full birod contact

Before considering any questions of applying moments we must first enforce the complete contact of both rods, as well as the unstreatchable nature of the two rods. To order ϵ both can be done using (D.19), enforcing **(69)** for both rods and demanding $s_{1c}(0) = s_{2c}(0)$. This allows us to eliminate the constants C_{14} and C_7, it will also introduce the length correction of the contact line $L_c = L^{(1)}$ to the system as an unknown. In section F it will be important to know the specific forms of C_7 and C_{14} which are

$$C_7 = -\frac{1}{2LR}\csc(\theta)\left(\frac{4R^3(C_8-C_9)\cos(\theta)\cos(2\theta)\cot(\theta)\sinh(2L\Theta_1)}{2\cos(2\theta)+\cos(4\theta)+3} + 2L_1\sec(\theta)\right), \tag{D.24}$$

$$C_{14} = \tag{D.25}$$

$$\frac{1}{8L(\cos(2\theta)+\cos(4\theta)+2)}R^2\csc^2(\theta)\sec^2(2\theta)\Bigg[\csc(\theta)\sin\left(\frac{L\tan(\theta)}{2R}\right)\Big(N_{2r}R(23\cos(2\theta)+15\cos(4\theta)+\cos(6\theta)+25)$$
$$-16C_{11}\sin(\theta)(\cos(\theta)+\cos(3\theta))^2\Big) - 2LN_{2r}(5\cos(\theta)+2\cos(3\theta)+\cos(5\theta))\cos\left(\frac{L\tan(\theta)}{2R}\right)\Bigg]$$

E Bending Response

Using the fact that the zeroth order effective rod curvatures U_{jr} are zero we substitute (D.7)-(D.8) into (43) and (44) to obtain

$$\mathsf{U}_{1r}(s) = \mathsf{U}_{1r}^{i}\sin\left(\frac{s\tan(\theta)}{R}\right) + \mathsf{U}_{1r}^{ii}\cos\left(\frac{2s\tan(\theta)}{R}\right) + \mathsf{U}_{1r}^{iii}\sin\left(\frac{2s\tan(\theta)}{R}\right) + \mathsf{U}_{1r}^{iv}s + \mathsf{U}_{1r}^{v}, \tag{E.1}$$

$$\mathsf{U}_{2r}(s) = \mathsf{U}_{2r}^{i}\cos\left(\frac{s\tan(\theta)}{R}\right) + \mathsf{U}_{2r}^{ii}\cos\left(\frac{2s\tan(\theta)}{R}\right) + \mathsf{U}_{2r}^{iii}\sin\left(\frac{2s\tan(\theta)}{R}\right) + \mathsf{U}_{2r}^{iv}s + \mathsf{U}_{2r}^{v}, \tag{E.2}$$

The case in which $\mathsf{N}_{1r} = \mathsf{N}_{2r} = 0$ is covered in Section 6.2 of the paper. We turn our attention to the case in which at least one of N_{1r} and N_{2r} is non-zero. Similar to the definition of average curvature we define the averaged effective moments to be

$$\bar{\mathsf{M}}_{jr} = \frac{1}{L}\int_{-L/2}^{L/2} \mathsf{M}_{jr}(q)\ \mathrm{d}q, j = 1, 2, 3. \tag{E.3}$$

Applying this to (D.21) we find

$$\bar{\mathsf{M}}_{1r} = -\frac{\csc(\theta)(4C_{13}(\sin(2\theta) + \sin(6\theta)) + \mathsf{N}_{1r}R(9\cos(\theta) + 6\cos(3\theta) + \cos(5\theta)))}{4(\cos(2\theta) + \cos(4\theta) + 2)}, \tag{E.4}$$

$$\bar{\mathsf{M}}_{2r} = -\frac{\csc(\theta)(\mathsf{N}_{2r}R(9\cos(\theta) + 6\cos(3\theta) + \cos(5\theta)) - 4C_{11}(\sin(2\theta) + \sin(6\theta)))}{4(\cos(2\theta) + \cos(4\theta) + 2)}. \tag{E.5}$$

Eliminating C_{13} for $\bar{\mathsf{M}}_{1r}$ and C_{11} for $\bar{\mathsf{M}}_{2r}$ we obtain

$$\begin{aligned}
&\bar{\mathsf{U}}_{1r} = \\
&\left(\frac{R\sec^2(2\theta)\left(-8L\sin(\theta) - 2L(2\sin(\theta) + \sin(3\theta))\cos\left(\frac{L\tan(\theta)}{R}\right) + R(\cos(2\theta) + \cos(4\theta) + 8)\sec(\theta)\sin\left(\frac{L\tan(\theta)}{R}\right)\right)}{16L}\right)\mathsf{N}_{1r} \\
&+ \left(\frac{\sec^2(2\theta)\left(L(\cos(3\theta) + \sec(\theta)) - R(2\sin(\theta) + \sin(3\theta))\sin\left(\frac{L\tan(\theta)}{R}\right)\right)}{4L}\right)\bar{\mathsf{M}}_{1r}.
\end{aligned}$$

Under the assumptions of Section 6.0.1 the leading order term in a series in R is

$$\bar{\mathsf{U}}_{1r} \approx \frac{1}{4}\sec^2(2\theta)(\cos(3\theta) + \sec(\theta))\bar{\mathsf{M}}_{1r} = \frac{1}{4}\left(\sec(\theta) + \cos(\theta)\sec^2(2\theta)\right)\bar{\mathsf{M}}_{1r}. \tag{E.6}$$

Leading to the same conclusion as in the case where the forces were absent. For U_{2r} we have

$$\begin{aligned}
&\bar{\mathsf{U}}_{2r} = \\
&\frac{1}{64L^2}\left(R\csc^2(\theta)\sec^2(2\theta)\left(L\left(8L\sin^3(\theta)\left((2\cos(2\theta) + 3)\cos\left(\frac{L\tan(\theta)}{R}\right) - 4\right)\right.\right.\right. \\
&\left.\left.\left. - R(\cos(2\theta) + \cos(4\theta) - \cos(6\theta) + 31)\sec(\theta)\sin\left(\frac{L\tan(\theta)}{R}\right)\right) - 64R^2\csc(\theta)\left(\cos\left(\frac{L\tan(\theta)}{R}\right) - 1\right)\right)\right)\mathsf{N}_{2r} \\
&+ \left(\frac{\sec^2(2\theta)\left(L^2(\cos(3\theta) + \sec(\theta)) + 4R^2\cot(\theta)\csc(\theta)\left(\cos\left(\frac{L\tan(\theta)}{R}\right) - 1\right) + LR\sin(\theta)(2\cos(2\theta) + 3)\sin\left(\frac{L\tan(\theta)}{R}\right)\right)}{4L^2}\right)\bar{\mathsf{M}}_{2r}.
\end{aligned}$$

Once again using assumptions of Section 6.0.1 the leading order term is

$$\bar{\mathsf{U}}_{2r} \approx \frac{1}{4}\left(\sec(\theta) + \cos(\theta)\sec^2(2\theta)\right)\bar{\mathsf{M}}_{2r}. \tag{E.7}$$

F Torsional Response

On applying the full contact constraint as discussed in Section D.3 we obtain

$$\mathsf{U}_{3r} = -\frac{L_c\csc(\theta)\sec(\theta)}{LR} + \mathsf{U}_{3r}^{i} + \mathsf{U}_{3r}^{ii}\left(C_8\,\mathrm{e}^{\Theta_1 s} - C_9\,\mathrm{e}^{-\Theta_1 s}\right), \tag{F.1}$$

With L_c the change in length of the contact line. The average $\bar{\mathsf{U}}_{3r}$ is

$$\bar{\mathsf{U}}_{3r} = -\frac{L_c\csc(\theta)\sec(\theta)}{LR}. \tag{F.2}$$

So we only require an expression for the contact line length correction L_c. Substituting (D.14) and (D.15), (D.20), (D.24) and (D.25) into (70) we obtain an expression for L_c in terms of the effective forces and moments, $\alpha_1^{\pm}$, $\alpha_2^{\pm}$ and the constants C_8 and C_9, which remain to be eliminated.

From (D.16) and (D.17), (D.24) and (D.25) we find the quantities $\beta_i(L/2) - \beta_i(-L/2)$, $i = 1, 2$ are identical, hence from (71) the quantities $\beta_i^{\pm}$ are also the same. Also they only depend on the constant C_7, which from (D.24) means they only depend on the sum $C_8 + C_9$ and we can eliminate both for $\beta^{\pm}$. Thus by applying the condition (71) we obtain (85). This is also sufficient to determine the averaged birod twist $\bar{\mathsf{U}}_{3r}$. In passing we note that the actual twist U_{3r} also depends on the difference $C_8 - C_9$ and would require specification of further geometric quantities.

G Derivation of the Linear Torsional and Extensional Response of A Uniform Helical Birod

Multiplying (57) by $\cos(\theta)$ we obtain

$$\frac{\partial \phi}{\partial s_i} = \frac{\sec(2\theta)(R(\mathsf{M}_{3r}\cos(\theta) - \mathsf{N}_{3r}R\sin(\theta)) - 2\sin(\theta)\cos(\theta)((\gamma-1)\cos(2\theta)+1))}{2\gamma R}. \tag{G.1}$$

Under the boundary constraints for which the angles α_i are fixed at the birod ends for all deformations the left hand side must be constant with respect to all deformation sets $\mathcal{P}$ (M_{3r} and N_{3r} here). This is a result of the fact that the rod's lengths L_r are fixed and that $\frac{\partial \phi}{\partial s_i}$ is constant in any given admissible helical configuration. With this the twist rate is given by $(\phi(L/2)-\phi(-L/2))/L_i$ and if α_i are fixed at the boundaries for all admissible configurations it is a fixed quantity. Taking the partial derivative of (G.1) with respect to M_{3r} and evaluating at $\mathsf{M}_{3r}=0, \mathsf{N}_{3r}=0$ we obtain

$$0 = \frac{R\cos(\theta)\sec(2\theta) - 2\frac{\partial\theta}{\partial \mathsf{M}_{3r}}\left((\gamma-1)\cos(2\theta)+\sec^2(2\theta)\right)}{2\gamma R}. \tag{G.2}$$

giving us an expression for $\frac{\partial\theta}{\partial \mathsf{M}_{3r}}$ in terms of the original angle θ. Since $\mathsf{U}_3 = \tan(\theta)/R$ we have

$$\frac{\partial \mathsf{U}_3}{\partial \mathsf{M}_{3r}} = \frac{\sec^2(\theta)}{R}\frac{\partial\theta}{\partial \mathsf{M}_{3r}} = \frac{\sec(\theta)}{2\left((\gamma-1)\cos^2(2\theta)+\sec(2\theta)\right)}.$$

using (G.2). The inverse of this is the coefficient of linear response of the uniformly helical birod and it is the same as (87).

Taking the partial derivatives of (G.1) with respect to N_{3r} and evaluating at $\mathsf{M}_{3r}=0, \mathsf{N}_{3r}=0$ we obtain

$$0 = -\frac{\sec^2(2\theta)\left(\frac{\partial\theta}{\partial \mathsf{N}_{3r}}(3(\gamma-1)\cos(2\theta)+(\gamma-1)\cos(6\theta)+4) + R^2(\sin(3\theta)-\sin(\theta))\right)}{4\gamma R} \tag{G.3}$$

Using this we obtain

$$\frac{\partial \mathsf{u}_3}{\partial \mathsf{N}_{3r}} = \frac{\sec^2(\theta)}{R}\frac{\partial\theta}{\partial \mathsf{N}_{3r}} = -\frac{2R\cos(2\theta)\tan(\theta)\sec(\theta)}{3(\gamma-1)\cos(2\theta)+(\gamma-1)\cos(6\theta)+4}.$$

It can be confirmed that the inversion of this gives (88).

The relative extension of the contact line, by comparison to its zero force and moment equilibrium length is given by

$$\mathrm{e} = \frac{L_i\cos(\theta^*)}{L_i\cos(\theta)}$$

With θ^* the deformed helical angle. It is only θ^* which is a function of M_{3r} and N_{3r} here. Taking derivatives evaluated at $\mathsf{M}_{3r}=\mathsf{N}_{3r}=0$ we have

$$\frac{\partial e}{\partial \mathsf{M}_{3r}} = -\tan(\theta)\frac{\partial\theta}{\partial \mathsf{M}_{3r}}, \quad \frac{\partial e}{\partial \mathsf{N}_{3r}} = -\tan(\theta)\frac{\partial\theta}{\partial \mathsf{N}_{3r}}.$$

substituting for the partial derivatives obtained from (G.2) and (G.3) we obtain

$$\frac{\partial e}{\partial \mathsf{M}_{3r}} = -\frac{R\sin(\theta)\sec(2\theta)}{2\left((\gamma-1)\cos(2\theta)+\sec^2(2\theta)\right)}, \quad \frac{\partial e}{\partial \mathsf{N}_{3r}} = \frac{2R^2\sin(\theta)\cos(2\theta)\tan(\theta)}{3(\gamma-1)\cos(2\theta)+(\gamma-1)\cos(6\theta)+4},$$

whose inversions give the coefficients of (90).

References

1. Antman S: Nonlinear Problems of Elasticity, 2nd ed. New York, Springer-Verlag (p 265) (1995).
2. Argatov I.,: Response of a wire rope strand to axial and torsional loads: Asymptotic modeling of the effect of inter-wire contact deformations, **48**, 1413-1423 (2011).
3. Asghari-Targhi M., and Berger M. A.: Writhe in the stretch-twist-fold dynamo. Geophys. Astrophys. Fluid Dyn. **103**, 69-87 (2009).
4. Balaeff A., Kourdella C. R., Mahadevan L., Schulten K.: Modelling DNA loops using continuum and statistical mechanics. Phil. Trans. R. Soc. Lond. A **362**, 1355-1371 (2004).
5. Banavar J. R., Maritan A., Micheletti C., Trovato A.: Geometry and physics of proteins. Proteins: Struct. Func. Genet, **47**, 315-322 (2002).
6. Banavar J. R., Maritan A.: Physics of proteins. Ann. Rev. Biophys. Biomol. Struct. **36**, 261-280 (2007)
7. Banavar J. R., Cieplak M., Flammini A., Hoang T. X., Kamien R. D., Lezon T., Marenduzzo D., Maritan A., Seno F., Snir Y., Trovato A : Geometry of proteins: Hydrogen bonding, sterics and marginally compact tubes. Phys. Rev. E. **73**, 031921(1-5) (2006).
8. Bouchiat C., Meźard M.: An elastic rod model of a super-coiled DNA molecule. Eur. Phys. J. **2**, 377-402 (2000).
9. Coleman B. D., Swigon D.: Theory of super-coiled elastic rings with self-contact and its application to plasmids, J. Elast. **60** 173-221 (2000).
10. Costello G. A.: Large deflections of helical spring due to bending. J. Eng. Mech. Div. boldmath103, 481-487 (1997).

11. Costello G. A.: Theory of Wire Rope. New York, Springer-verlag (1997).
12. Elata D., Eshkenazy R., Weiss M. P.: The mechanical behavior of a wire rope with an independent wire rope core. Intl. J. Solids Struct. **41** 1157-1172 (2004).
13. Ghoreishia S. R., Messager T. Cartraud P. Davies P.: Validity and limitations of linear analytical models for steel wire strands under axial loading, using a 3D FE model. J. Mech. Sci. **49**, 1251-1261 (2007)
14. Ghoreishia S. R., Cartrauda P., Davies P., Messeger T.: Analytical modeling of synthetic fiber ropes subjected to axial loads. Part I: A new continuum model for multilayered fibrous structures. Intl, J. Solids Struct. **44**, 29242942 (2007)
15. Gittes F, Mickey B, Nettleton J, Howard J.: Flexural rigidity of microtubules and Actin filaments measured from thermal fluctuations in shape. J. Cell Biol. **120**, 923-934 (1993)
16. Ghoreishia S. R., Davies P., Cartraud P., Messager T., Analytical modeling of synthetic fiber ropes. Part II: A linear elastic model for 1 + 6 fibrous structures. Intl. J. Solids Struct. **44**, 29432960 (2007)
17. Goriely A., Tabor M.: Nonlinear dynamics of filaments I: Dynamical instabilities. Physica D. **105**, 45-61 (1997)
18. Goriely A., Nizette M., Tabor.: On the dynamics of elastic strips. J. Nonlinear Sci. **11**, 3-45 (2001).
19. Healy T. J.: A rigorous derivation of hemitropy in nonlinearly elastic rods. Disc. Cont. Dyn. Sys. B. **16**, 265 -282 (2011).
20. Jiang W. G., Warby M. K., Henshall J. L.: Statically indeterminate contacts in axially loaded wire strand. European J. Mech A: Solids. **27** , 69- 78 (2008).
21. Kerhbaum S. Maddocks J. H.: Effective properties of elastic rods with high intrinsic twist. in M. Deville and R. Owens, editors, Proc. of the 16th IMACS World Congress 2000", 1-8 (2000)
22. Kreplak L., Br H., Leterrier J. F., Herrmann H., Aebi U.: 2005, Exploring the mechanical behavior of single intermediate filaments. J. Mol. Biol. **354**, 569-577 (2005)
23. Kreplak L., Herrmann H., Aebi U.: Tensile properties of single domain intermediate filaments. Biophys. J. **94**, 2790-2792 (2008)
24. Kumar K. Cochran J. E.: Closed-form analysis for elastic deformations of multilayered strands. J. Appl. Mech. **54**, 898-. (1987)
25. Kreyszig E: Differential Geometry:Chapter II. Dover Publications, New York (1991).
26. Moakher M. Maddocks J.: A double-strand elastic rod theory. Arch. Rat. Mech. Anal. **177**, 53-91 (2005)
27. Morimoto T., Iizuka H.: Self-equilibrium configurations of composite strands. Compos. struct. **94**, 15751581 (2012)
28. Neukirch S. Goriely A. Hausrath A.: Elastic coiled-coils act as energy buffers in the ATP synthase. Intl. J. Non-linear Mech. **43**, 1064-1073 (2008)
29. Neukirch S. van der Heijden G.: Geometry and Mechanics of uniform n-plies: from engineering ropes to biological filaments. J. Elast. **69**, 41-72 (2002).
30. Nizette M. Goriely A.: Towards a classification of Euler-Kirchhoff filaments. J. Math. Phys. **40**, 2830-2866 (1999)
31. Przybyl S. Pierański P.: Helical close packing of ideal ropes. Eur. Phys. J. E. **4**, 445-449 (2001)
32. Ramsay H.: A Theory of thin rods with application to helical constituent wires in cables. Intl. J. Mech. Sci. **30**, 559570 (1988)
33. Ramsay H.: Analysis of interwire friction in multilayered cables under uniform extension and twisting. Intl. J. Mech. Sci. **32**, 709716 (1990)
34. Raoof M., Hobbs R. E.: Analysis of multilayered structural strands. J. Eng. Mech. **114**, 1166-1182 (1988)
35. Root D. D., Yadavalli V. K., Forbes J. G., Wang K.: Coiled-coil nanomechanics and uncoiling and unfolding of the superhelix and -Helices of Myosin. Biophys. J. **90**, 2852-2866 (2006)
36. Rose A., Meier I.: Scaffolds, levers, rods and springs: Diverse cellular functions of long coiled-coil Proteins. Cell. Mol. Life Sci. **61**, 19962009 (2004)
37. Sathikh S., Moorthy M. B. K., Krishnan M.: Symmetric linear elastic model for helical wire strands under axisymmetric loads. J. Strain Anal. Eng. Des. **31**, 389-99 (1996)
38. Schwaiger I., Sattler C., Hostetter D. R., Rief M. The Myosin coiled-coil is a truly elastic protein structure. Nat. Mater. **1**, 232-235 (2002)
39. Smith S. B. Finzi L. Bustamante C.: Direct mechanical measurements of the elasticity of single DNA molecules by using magnetic beads. Science. **258**, 1122-1126 (1992).
40. Staple D. B., Loparic M., Kreuzer H. J., Kreplak L.: Stretching, unfolding, and deforming protein filaments adsorbed at Solid-Liquid interfaces using the tip of an atomic-force microscope. Phys. Rev. Lett. **102**, 128302 (2009)
41. Starostin E. L., van der Heijden G. H. M.: Theory of equilibria of elastic 2-braids with interstrand interation. J Mech. Phys. Solids, *In Press*.
42. Tatsuya H.: SMC proteins and chromosome mechanics : from bacteria to humans. Philos. trans. Royal Soc. London. **29**, 507-514 (2005)
43. Thompson J. M. T. van der Heijden G. Neukirch S.: Super-coiling of DNA plasmids: mechanics of the generalised ply. Proc. R. Soc. London. A. **458**, 959-985 (2002)
44. Tobias I. Swigon D. Coleman B. D. Elastic stability of DNA configurations, I , general theory. Phys. Rev. E. **61**, 747-758 (2000)
45. Tsuda Y, Yasutake H, Ishijima A, Yanagida T.: Torsional rigidity of single actin filaments and actinactin bond breaking force under torsion measured directly by in vitromicromanipulation. Proc. Natl. Acad. Sci. 93, 1293712942 (1996).
46. Usabiaga H., Pagalday J. M.: Analytical procedure for modelling recursively and wire by wire stranded ropes subjected to traction and torsion loads. **45**, 5503-5520 (2008)
47. van der Heijden G., Thompson J. M. T., Neukirch S.: A variational approach to loaded ply structures. J. Vib. Control. **9**, 175-185 (2003)
48. Velinsky S. A.: General nonlinear theory for complex wire rope. J. Mech. Sci. **27**, 497507 (1985)
49. Vologodskii A. V., Marko J. F.: Extension of torsionally stretched DNA by external force. Biophys. J. **73(1)**, 123-132 (1997)
50. Yogurtcu O. N., Kim J.S., Sun S.X.: A Mechanochemical Model of Actin Filaments. Biophys. J. **103**, 719727 (2012)